Numerical Verification of the Hasselmann equation.

A.O. Korotkevich[1], A. Pushkarev[2,5], D. Resio[4], V.E. Zakharov[3,2,1,5]
[1]L.D. Landau Institute for Theoretical Physics RAS, Moscow
[2]P.N. Lebedev Physical Institute RAS, Moscow
[3]Department of Mathematics, University of Arizona, Tucson,
[4]Coastal and Hydraulics Laboratory,
U.S. Army Engineer Research and Development Center, Vicksburg
[5]Waves and Solitons LLC, Phoenix

July 19, 2006

Abstract

Theory of weak turbulence is designed for statistical description of weakly-nonlinear wave ensembles in media with dispersion. The main tool of weak turbulence theory is kinetic equation for squared wave amplitudes, or a system of such equations. Since the discovery of the kinetic equation for bosons by Nordheim (1928) and also paper by Peierls (1929) in the context of solid state physics, this quantum-mechanical tool was applied to wide variety of classical problems, including wave turbulence in hydrodynamics, plasmas, liquid helium, nonlinear optics, etc.

Such kinetic equations have rich families of exact solutions describing weak-turbulent Kolmogorov spectra. Also, kinetic equations for waves have self-similar solutions describing temporal or spatial evolution of weak – turbulent spectra.

However, one of the most remarkable example of weak turbulence is wind-driven sea. The kinetic equation describing statistically the gravity waves on the surface of ideal liquid was derived by Hasselmann (1962). Since this time the Hasselmann equation is widely used in physical oceanography as foundation for development of wave-prediction models: WAM, SWAN and WAVEWATCH.

In spite of tremendous popularity of the Hasselmann equation, its validity and applicability for description of real wind-driven sea has never been completely proven. It was criticized by many respected authors, not only in the context of oceanography.

The verification of the weak turbulent theory is an urgent problem, important for the whole physics of nonlinear waves. The verification can be done by direct numerical simulation of the primitive dynamical equations describing wave turbulence in nonlinear medium.

In this article we present results of new seria of numerical experiments on modelling of swell propagation withing frameworks of both dynamical and kinetic equations. In this case we used fine anisotropic grid containing 512×4096 modes. We think that our results can be considered as first direct verification of wave kinetic equation.

Problem formulation

Let us consider a potential flow of an ideal fluid of infinite depth with a free surface. We use standard notations for velocity potential $\phi(\vec{r}, z, t), \vec{r} = (x, y); \vec{v} = \nabla\phi$ and surface elevation $\eta(\vec{r}, t)$. Fluid flow is incompressible $(\nabla\vec{v}) = \triangle\phi = 0$. The total energy of the system can be presented in the following form

$$H = T + U,$$

$$T = \frac{1}{2}\int d^2r \int\limits_{-\infty}^{\eta} (\nabla\phi)^2 dz, \qquad (1)$$

$$U = \frac{1}{2}g\int \eta^2 d^2r, \qquad (2)$$

here g is the gravity acceleration.

Hamiltonian expansion

It was shown by Zakharov (1966) that under these assumptions the fluid is a Hamiltonian system

$$\frac{\partial \eta}{\partial t} = \frac{\delta H}{\delta \psi}, \quad \frac{\partial \psi}{\partial t} = -\frac{\delta H}{\delta \eta}, \tag{3}$$

where $\psi = \phi(\vec{r}, \eta(\vec{r}, t), t)$ is a velocity potential on the surface of the fluid. In order to calculate the value of ψ we have to solve the Laplas equation in the domain with varying surface η. One can simplify the situation, using the expansion of the Hamiltonian in powers of "steepness"

$$\begin{aligned} H = &\frac{1}{2}\int \left(g\eta^2 + \psi\hat{k}\psi\right) d^2r + \\ +&\frac{1}{2}\int \eta \left[|\nabla\psi|^2 - (\hat{k}\psi)^2\right] d^2r + \\ +&\frac{1}{2}\int \eta(\hat{k}\psi)\left[\hat{k}(\eta(\hat{k}\psi)) + \eta\triangle\psi\right] d^2r. \end{aligned} \tag{4}$$

Dynamical equations

In this case dynamical equations acquire the following form

$$\begin{aligned}
\dot{\eta} &= \hat{k}\psi - (\nabla(\eta\nabla\psi)) - \hat{k}[\eta\hat{k}\psi] + \\
&\quad + \hat{k}(\eta\hat{k}[\eta\hat{k}\psi]) + \tfrac{1}{2}\triangle[\eta^2\hat{k}\psi] + \tfrac{1}{2}\hat{k}[\eta^2\triangle\psi], \\
\dot{\psi} &= -g\eta - \tfrac{1}{2}\left[(\nabla\psi)^2 - (\hat{k}\psi)^2\right] - \\
&\quad - [\hat{k}\psi]\hat{k}[\eta\hat{k}\psi] - [\eta\hat{k}\psi]\triangle\psi + D_{\vec{r}} + F_{\vec{r}}.
\end{aligned} \qquad (5)$$

Here $D_{\vec{r}}$ is some artificial damping term used to provide dissipation at small scales; $F_{\vec{r}}$ is a pumping term corresponding to external force (having in mind wind blow, for example). Let us introduce Fourier transform

$$\psi_{\vec{k}} = \frac{1}{2\pi}\int \psi_{\vec{r}} e^{i\vec{k}\vec{r}} d^2r, \quad \eta_{\vec{k}} = \frac{1}{2\pi}\int \eta_{\vec{r}} e^{i\vec{k}\vec{r}} d^2r.$$

Canonical variables

It is convenient to introduce the canonical variables $a_{\vec{k}}$ as shown below

$$a_{\vec{k}} = \sqrt{\frac{\omega_k}{2k}}\eta_{\vec{k}} + i\sqrt{\frac{k}{2\omega_k}}\psi_{\vec{k}}, \text{where } \omega_k = \sqrt{gk}. \tag{6}$$

With these variables the dynamical equations take the following form

$$\dot{a}_{\vec{k}} = -i\frac{\delta H}{\delta a^*_{\vec{k}}}. \tag{7}$$

$$
\begin{aligned}
&H_0 = \int \omega_k |a_{\vec{k}}|^2 \mathrm{d}\vec{k},\\
&H_1 = \frac{1}{6}\frac{1}{2\pi}\int E^{\vec{k}_0}_{\vec{k}_1\vec{k}_2}(a_{\vec{k}_1}a_{\vec{k}_2}a_{\vec{k}_0} + a^*_{\vec{k}_1}a^*_{\vec{k}_2}a^*_{\vec{k}_0})\delta(\vec{k}_1+\vec{k}_2+\vec{k}_0)\mathrm{d}\vec{k}_1\mathrm{d}\vec{k}_2\mathrm{d}\vec{k}_0 +\\
&+\frac{1}{2}\frac{1}{2\pi}\int C^{\vec{k}_0}_{\vec{k}_1\vec{k}_2}(a_{\vec{k}_1}a_{\vec{k}_2}a^*_{\vec{k}_0} + a^*_{\vec{k}_1}a^*_{\vec{k}_2}a_{\vec{k}_0})\delta(\vec{k}_1+\vec{k}_2-\vec{k}_0)\mathrm{d}\vec{k}_1\mathrm{d}\vec{k}_2\mathrm{d}\vec{k}_0,\\
&H_2 = \frac{1}{4}\frac{1}{(2\pi)^2}\int W_{\vec{k}_1\vec{k}_2\vec{k}_3\vec{k}_4}(a_{\vec{k}_1}a_{\vec{k}_2}a_{\vec{k}_3}a_{\vec{k}_4} + a^*_{\vec{k}_1}a^*_{\vec{k}_2}a^*_{\vec{k}_3}a^*_{\vec{k}_4})\times\\
&\times\delta(\vec{k}_1+\vec{k}_2+\vec{k}_3+\vec{k}_4)\mathrm{d}\vec{k}_1\mathrm{d}\vec{k}_2\mathrm{d}\vec{k}_3\mathrm{d}\vec{k}_4 +\\
&+\frac{1}{4}\frac{1}{(2\pi)^2}\int F_{\vec{k}_1\vec{k}_2\vec{k}_3\vec{k}_4}(a^*_{\vec{k}_1}a_{\vec{k}_2}a_{\vec{k}_3}a_{\vec{k}_4} + a_{\vec{k}_1}a^*_{\vec{k}_2}a^*_{\vec{k}_3}a^*_{\vec{k}_4})\times\\
&\times\delta(\vec{k}_1-\vec{k}_2-\vec{k}_3-\vec{k}_4)\mathrm{d}\vec{k}_1\mathrm{d}\vec{k}_2\mathrm{d}\vec{k}_3\mathrm{d}\vec{k}_4 +\\
&+\frac{1}{4}\frac{1}{(2\pi)^2}\int D_{\vec{k}_1\vec{k}_2\vec{k}_3\vec{k}_4}(a_{\vec{k}_1}a_{\vec{k}_2}a^*_{\vec{k}_3}a^*_{\vec{k}_4}\delta(\vec{k}_1+\vec{k}_2-\vec{k}_3-\vec{k}_4)\mathrm{d}\vec{k}_1\mathrm{d}\vec{k}_2\mathrm{d}\vec{k}_3\mathrm{d}\vec{k}_4.
\end{aligned}
\tag{8}
$$

The dispersion relation in the case of gravity waves on a deep water is of the "non-decay type" and equations

$$
\omega_{k_1} = \omega_{k_2} + \omega_{k_3}, \quad \vec{k}_1 = \vec{k}_2 + \vec{k}_3 \tag{9}
$$

have no real solution. It means that in the limit of small nonlinearity, the cubic terms in the Hamiltonian can be excluded by a proper canonical transformation $a(\vec{k},t) \longrightarrow b(\vec{k},t)$.

$$\begin{aligned}
&H_0 = \int \omega_k |b_{\vec{k}}|^2 \mathrm{d}\vec{k}, \\
&H_1 = 0, \\
&H_2 = \frac{1}{2}\frac{1}{(2\pi)^2}\int T_{\vec{k}_1\vec{k}_2\vec{k}_3\vec{k}_4}(b^*_{\vec{k}_1} b^*_{\vec{k}_2} b_{\vec{k}_3} b_{\vec{k}_4} \delta(\vec{k}_1+\vec{k}_2-\vec{k}_3-\vec{k}_4)\mathrm{d}\vec{k}_1\mathrm{d}\vec{k}_2\mathrm{d}\vec{k}_3\mathrm{d}\vec{k}_4.
\end{aligned} \tag{10}$$

Pair correlation functions

For statistical description of a stochastic wave field one can use a pair correlation function

$$< a_{\vec{k}} a^*_{\vec{k}'} >= n_k \delta(\vec{k} - \vec{k}'). \tag{11}$$

The $n_{\vec{k}}$ is measurable quantity, connected directly with observable correlation functions. For instance, from $a_{\vec{k}}$ definition one can get

$$I_k =< |\eta_{\vec{k}}|^2 >= \frac{1}{2}\frac{\omega_k}{g}(n_k + n_{-k}). \tag{12}$$

In the case of gravity waves it is convenient to use another correlation function

$$< b_{\vec{k}} b^*_{\vec{k}'} >= N_k \delta(\vec{k} - \vec{k}'). \tag{13}$$

The function N_k cannot be measured directly.

Kinetic equation

The relation connecting n_k and N_k is very simple (in the case of deep water)

$$\frac{n_k - N_k}{n_k} \simeq \mu, \tag{14}$$

where $\mu = (ka)^2$, here a is a characteristic elevation of the free surface. In the case of the weak turbulence $\mu \ll 1$.
The correlation function N_k obey the kinetic equation (Nordheim,1929; Hasselmann, 1962; Zakharov, 1966)

$$\frac{\partial N_k}{\partial t} = st(N, N, N) + f_p(k) - f_d(k), \tag{15}$$

Here

$$st(N,N,N) = 4\pi \int \left| T_{\vec{k},\vec{k}_1,\vec{k}_2,\vec{k}_3} \right|^2 \times \\ \times (N_{k_1} N_{k_2} N_{k_3} + N_k N_{k_2} N_{k_3} - N_k N_{k_1} N_{k_2} - \\ - N_k N_{k_1} N_{k_3}) \delta(\vec{k} + \vec{k}_1 - \vec{k}_2 - \vec{k}_3) d\vec{k}_1 d\vec{k}_2 d\vec{k}_3. \qquad (16)$$

Kolmogorov solutions

Let us consider stationary solutions of the kinetic equation assuming that

- The medium is invariant with respect to rotations;
- Dispersion relation is a power-like function $\omega = ak^{\alpha}$;
- $T_{\vec{k},\vec{k}_1,\vec{k}_2,\vec{k}_3}$ is a homogeneous function: $T_{\epsilon\vec{k},\epsilon\vec{k}_1,\epsilon\vec{k}_2,\epsilon\vec{k}_3} = \epsilon^{\beta} T_{\vec{k},\vec{k}_1,\vec{k}_2,\vec{k}_3}$.

Under this assumptions one can get Kolmogorov solutions

$$\begin{aligned} n_k^{(1)} &= C_1 P^{1/3} k^{-\frac{2\beta}{3}-d}, \\ n_k^{(2)} &= C_2 Q^{1/3} k^{-\frac{2\beta-\alpha}{3}-d}. \end{aligned} \tag{17}$$

Here d is a spatial dimension ($d = 2$ in our case). In the case of deep water $\omega = \sqrt{gk}$ and, apparently, $\beta = 3$.

Kolmogorov solutions (deep water)

It is known since (Zakharov and Filonenko, 1967) that on deep water

$$n_k^{(1)} = C_1 P^{1/3} k^{-4}. \tag{18}$$

In the same way (Zakharov, 1968) for second spectrum

$$n_k^{(2)} = C_2 Q^{1/3} k^{-23/6}. \tag{19}$$

Here we will explore the first spectrum (energy cascade):

$$I_k = \frac{C_1 g^{1/2} P^{1/3}}{k^{7/2}}. \tag{20}$$

Numerical simulation

Let us recall dynamical equations

$$
\begin{aligned}
\dot{\eta} &= \hat{k}\psi - (\nabla(\eta\nabla\psi)) - \hat{k}[\eta\hat{k}\psi]+ \\
&\quad +\hat{k}(\eta\hat{k}[\eta\hat{k}\psi]) + \frac{1}{2}\triangle[\eta^2\hat{k}\psi] + \frac{1}{2}\hat{k}[\eta^2\triangle\psi], \\
\dot{\psi} &= -g\eta - \frac{1}{2}\left[(\nabla\psi)^2 - (\hat{k}\psi)^2\right] - \\
&\quad -[\hat{k}\psi]\hat{k}[\eta\hat{k}\psi] - [\eta\hat{k}\psi]\triangle\psi + D_{\vec{r}} + F_{\vec{r}}.
\end{aligned}
\tag{21}
$$

To solve these equations one can use splitting method. Let us represent some dynamical equation in the following form

$$\dot{\psi} = R_{nl}(\eta, \psi) - \gamma_k \psi_{\vec{k}} + f_k$$

Splitting method

$$\dot{\psi} = R_{nl}(\eta, \psi) - \gamma_k \psi_{\vec{k}} + f_k$$

On one time step τ we can use the following scheme

$$\left[\begin{array}{c} \dot{\psi}^{(1)}_{\vec{k}} = R_{nl}(\eta^{(1)}_{\vec{k}}, \psi^{(1)}_{\vec{k}}), \\ \text{initial conditions} \\ \psi^{(0)}_{\vec{k}}, \eta^{(0)}_{\vec{k}} \end{array}\right] \longrightarrow \left[\begin{array}{c} \dot{\psi}^{(2)}_{\vec{k}} = -\gamma_k \psi^{(2)}_{\vec{k}}, \\ \text{initial conditions} \\ \psi^{(1)}_{\vec{k}}, \eta^{(1)}_{\vec{k}} \end{array}\right] \longrightarrow \left[\begin{array}{c} \dot{\psi}_{\vec{k}} = f_k, \\ \text{initial conditions} \\ \psi^{(2)}_{\vec{k}}, \eta^{(2)}_{\vec{k}} \end{array}\right]$$

$$\left[\begin{array}{c} \text{HIA,} \\ \text{result} \\ \psi^{(1)}_{\vec{k}}, \eta^{(1)}_{\vec{k}} \end{array}\right] \longrightarrow \left[\begin{array}{c} \psi^{(2)}_{\vec{k}} = \psi^{(1)}_{\vec{k}} \exp(-\gamma_k \tau), \\ \text{result} \\ \psi^{(2)}_{\vec{k}}, \eta^{(2)}_{\vec{k}} \end{array}\right] \longrightarrow \left[\begin{array}{c} \psi_{\vec{k}} = \psi^{(1)}_{\vec{k}} + f_k \tau, \\ \text{result} \\ \psi_{\vec{k}}, \eta_{\vec{k}} \end{array}\right]$$

Hamiltonian integration algorithm (HIA)

Let us consider difference of Hamiltonian function from n-th to $(n+1)$-th steps. Time step is equal to τ.

$$\frac{\Delta H}{\tau} = \frac{H^{n+1} - H^n}{\tau} = \frac{\delta H}{\delta \psi}\frac{\psi^{n+1} - \psi^n}{\tau} + \frac{\delta H}{\delta \eta}\frac{\eta^{n+1} - \eta^n}{\tau} = 0. \quad (22)$$

Here ΔH represents difference from one step to another.

$$\begin{aligned} \frac{\eta^{n+1} - \eta^n}{\tau} &= \frac{\delta H}{\delta \psi}[\eta^n, \eta^{n+1}, \psi^n, \psi^{n+1}], \\ \frac{\psi^{n+1} - \psi^n}{\tau} &= -\frac{\delta H}{\delta \eta}[\eta^n, \eta^{n+1}, \psi^n, \psi^{n+1}]. \end{aligned} \quad (23)$$

Iteration scheme

One can rewrite numerical scheme

$$\begin{aligned} \eta_{\vec{k}}^{n+1} &= A(k,\tau)\eta_{\vec{k}}^{n} + B(k,\tau)\psi_{\vec{k}}^{n} + C(k,\tau)R_{\eta} + D(k,\tau)R_{\psi}, \\ \psi_{\vec{k}}^{n+1} &= E(k,\tau)\eta_{\vec{k}}^{n} + A(k,\tau)\psi_{\vec{k}}^{n} + F(k,\tau)R_{\eta} + C(k,\tau)R_{\psi}, \end{aligned} \tag{24}$$

Let us introduce $\eta_{\vec{k}}^{n+1,s}$, here s is an iteration number.

- $s = 0 : \ \eta_{\vec{k}}^{n};$
- $s = 1 : \ (\eta_{\vec{k}}^{n+1} := \eta_{\vec{k}}^{n}) \longrightarrow \eta_{\vec{k}}^{n+1,1};$
- $s = 2 : \ (\eta_{\vec{k}}^{n+1} := \eta_{\vec{k}}^{n+1,1}) \longrightarrow \eta_{\vec{k}}^{n+1,2};$
- ...

Iteration scheme convergence control

One can get from dynamical equations the following part

$$\dot{\psi} = -g\eta - \frac{1}{2}(\nabla\psi)^2 + ...$$

Let us introduce N — number of iterations for desirable accuracy, N_{max} — maximum numbers of iterations acceptable, N_{min} — minimum numbers of iterations acceptable. Rule is the following ($\zeta < 1$)

$$\begin{array}{rll} \text{IF} & N > N_{max} & \tau = \zeta\tau; \\ \text{ELSE IF} & N < N_{min} & \tau = \tau/\zeta; \\ \text{ELSE} & & \tau = \tau. \end{array}$$

Direct cascade. Numerical scheme parameters

Let us add damping and pumping in dynamical equations

$$\begin{aligned} \dot{\eta}_{\vec{k}} &= ... - \gamma_k \eta_{\vec{k}}, \\ \dot{\psi}_{\vec{k}} &= ... - \gamma_k \psi_{\vec{k}} + F_k. \end{aligned} \tag{25}$$

$$\begin{aligned} F_k &= f_k e^{i R_{\vec{k}}(t)}, \\ f_k &= 4 F_0 \frac{(k - k_{p1})(k_{p2} - k)}{(k_{p2} - k_{p1})^2}; \\ D_{\vec{k}} &= \gamma_k \psi_{\vec{k}}, \\ \gamma_k &= -\gamma_1, k \leq k_{p1}, \\ \gamma_k &= -\gamma_2 (k - k_d)^2, k > k_d. \end{aligned} \tag{26}$$

Here $R_{\vec{k}}(t)$ — uniformly distributed random number in interval $(0, 2\pi)$. Simulation region $L_x = L_y = 2\pi$ with double periodic boundary conditions.

Pumping and damping parameters: $F_0 = 2 \times 10^{-4}, k_{p1} = 5,\ k_{p2} = 10.$

$$[128 \times 128, k_d = 32] \longrightarrow [256 \times 256, k_d = 64] \longrightarrow [512 \times 512, k_d = 128].$$

Direct cascade. Hamiltonian as a function of time

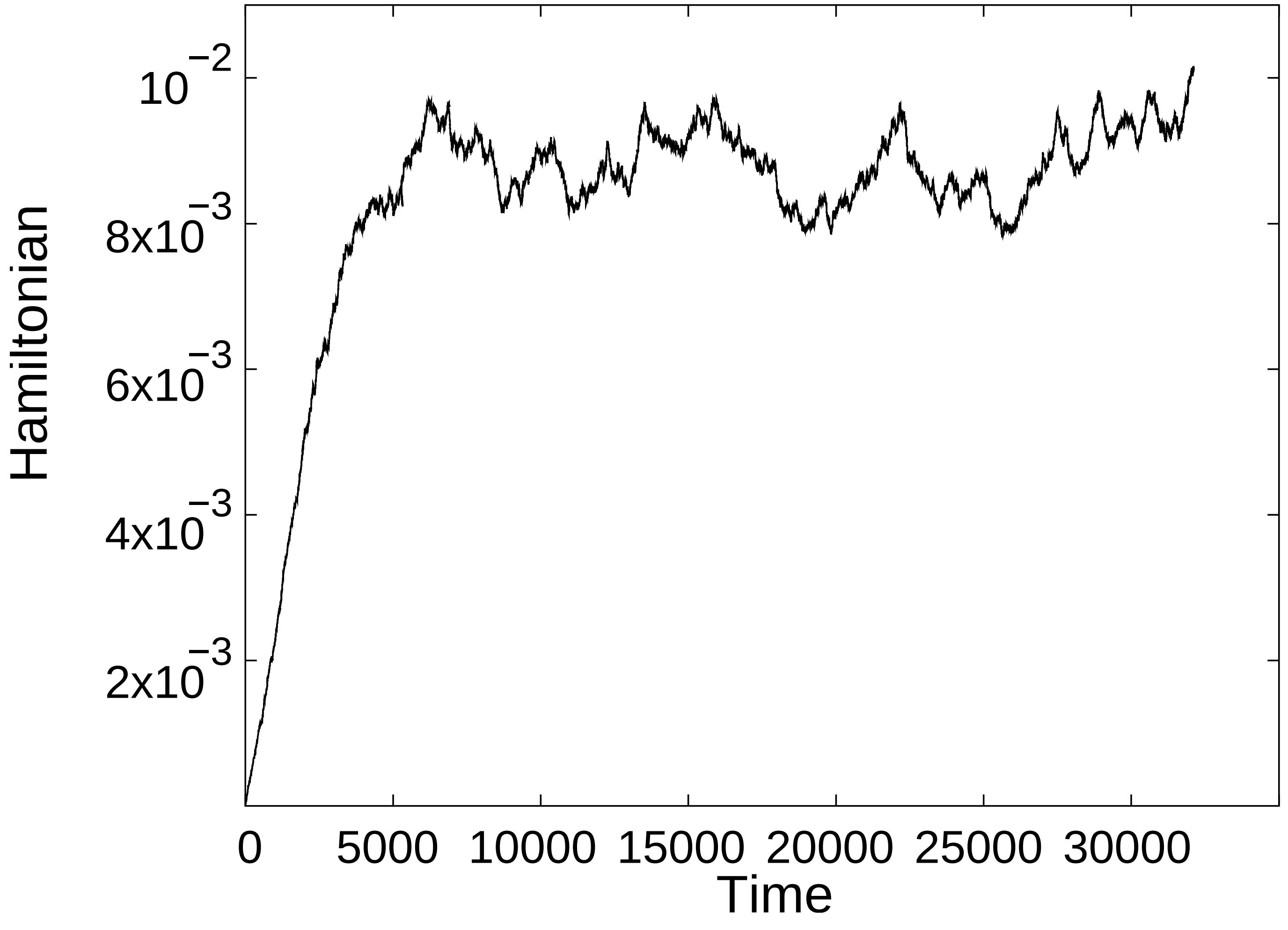

Direct cascade. Spectrum

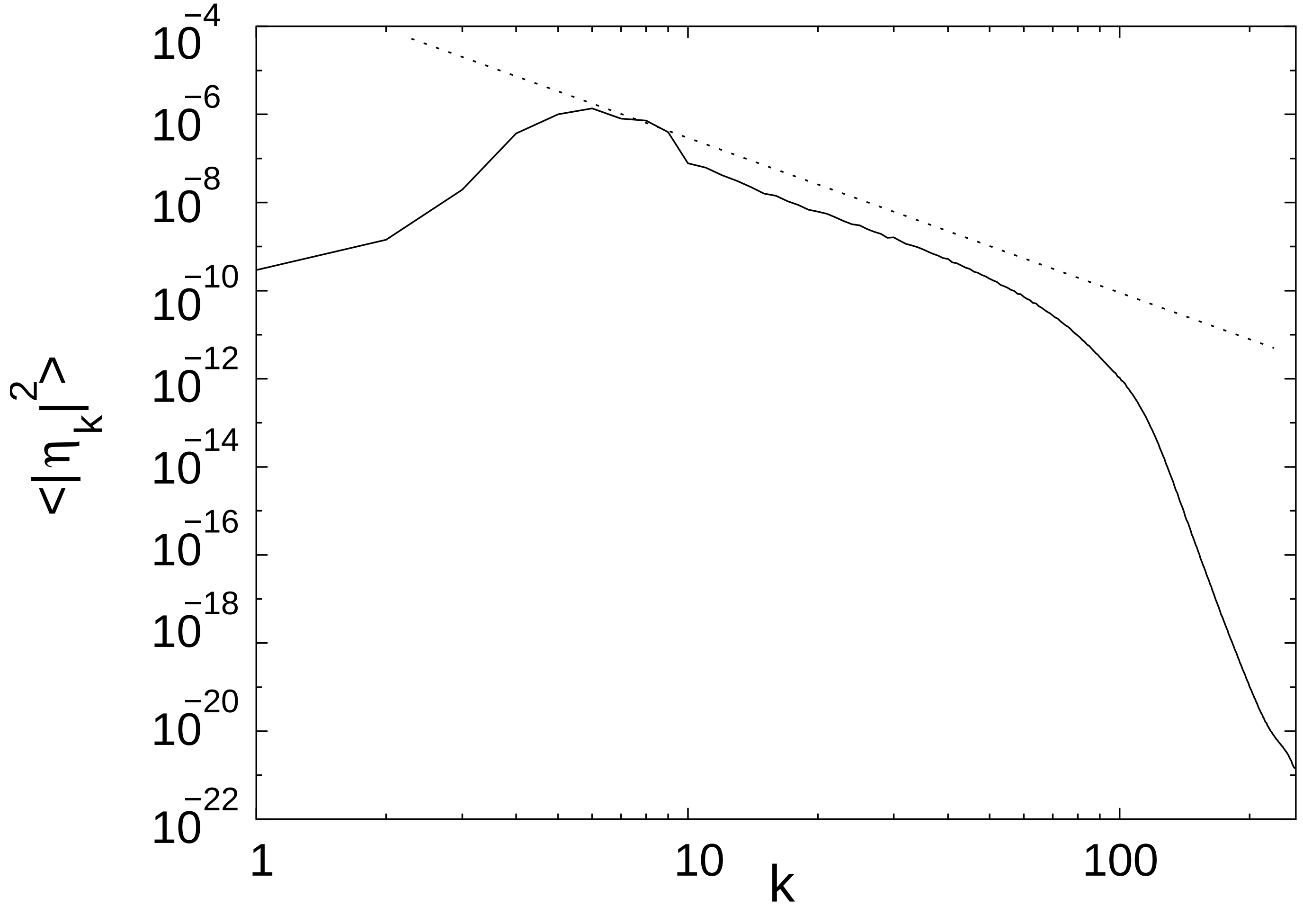

Direct cascade. Compensated spectra

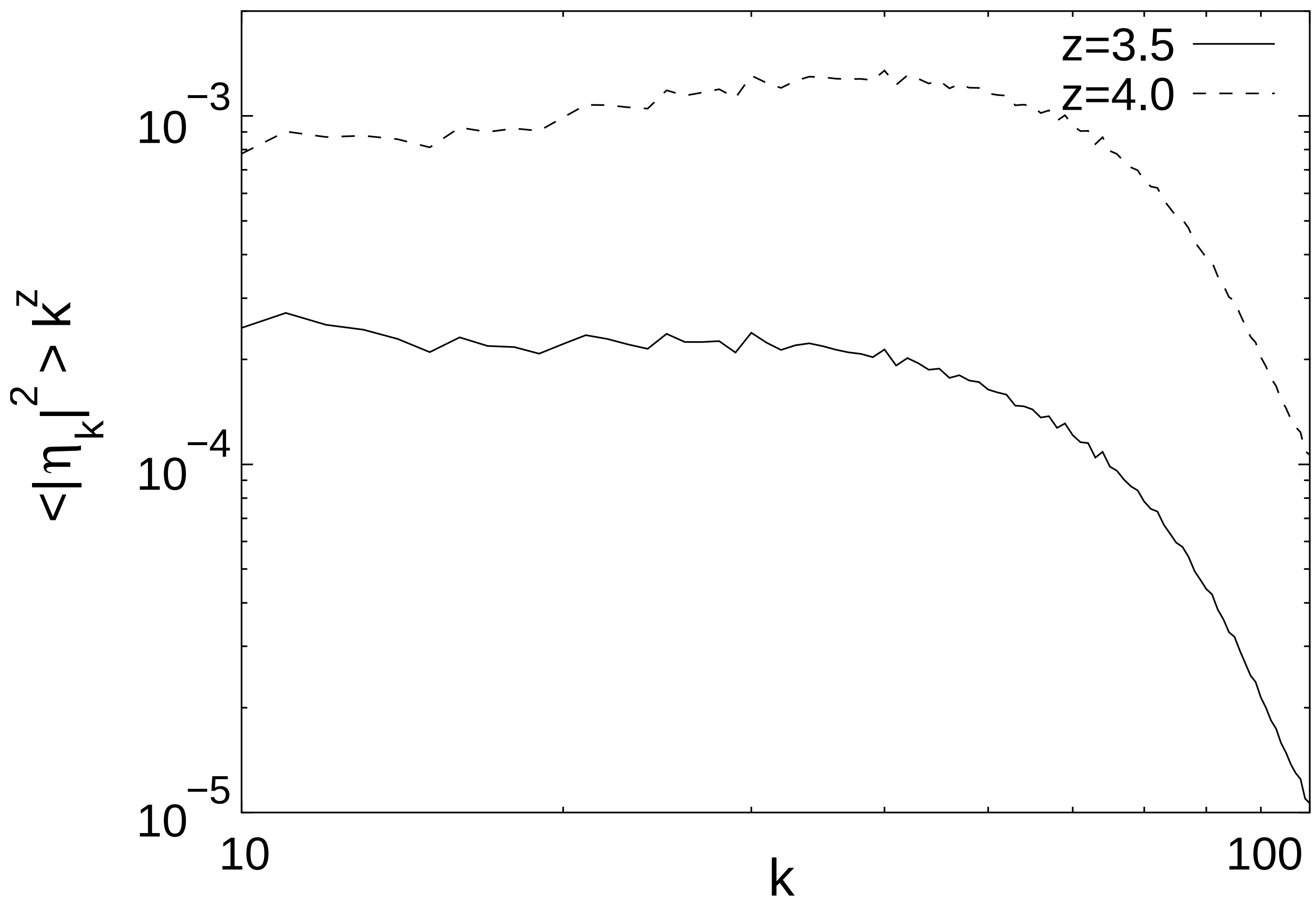

Direct cascade. Different grids

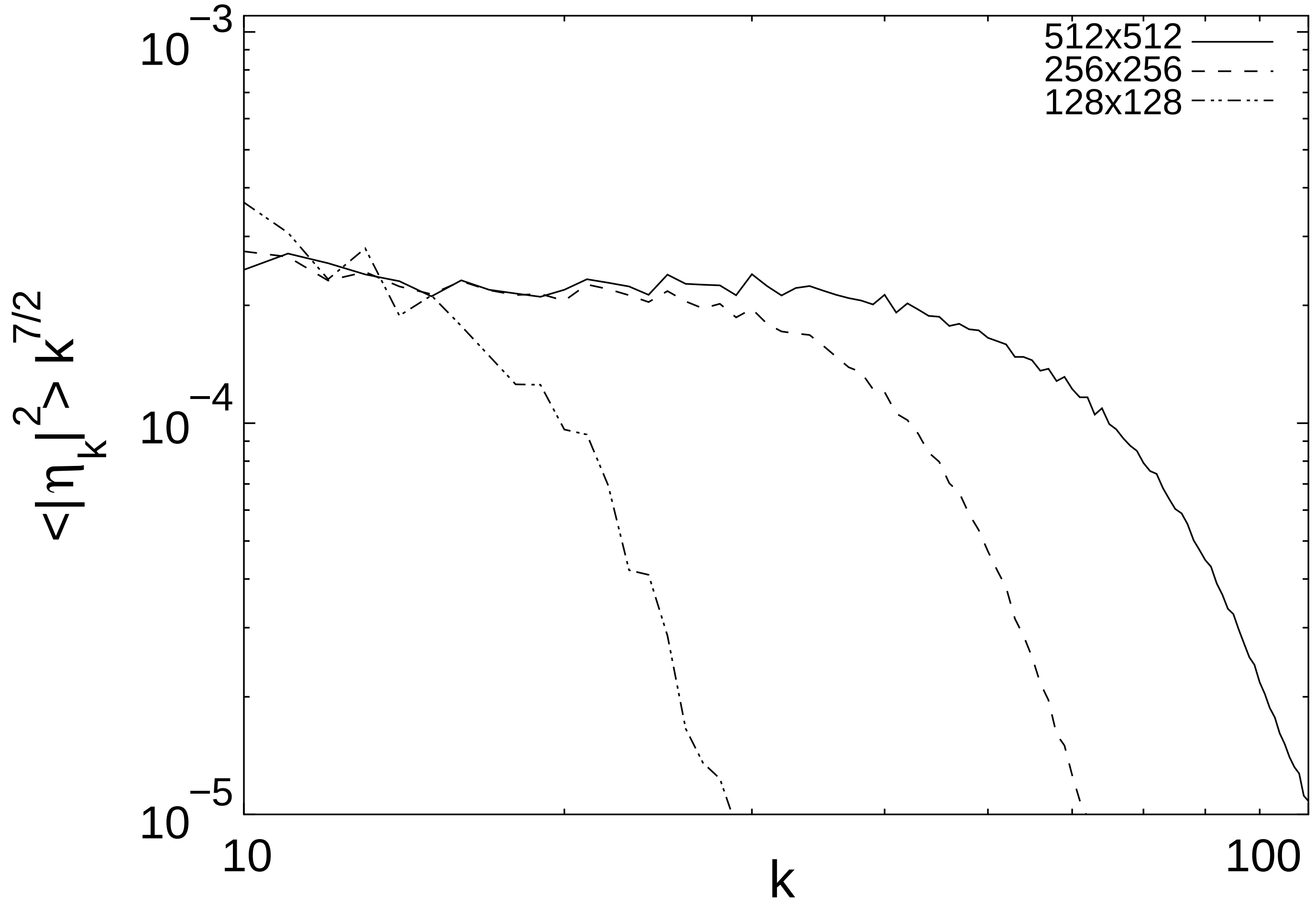

Direct cascade. Different pumping

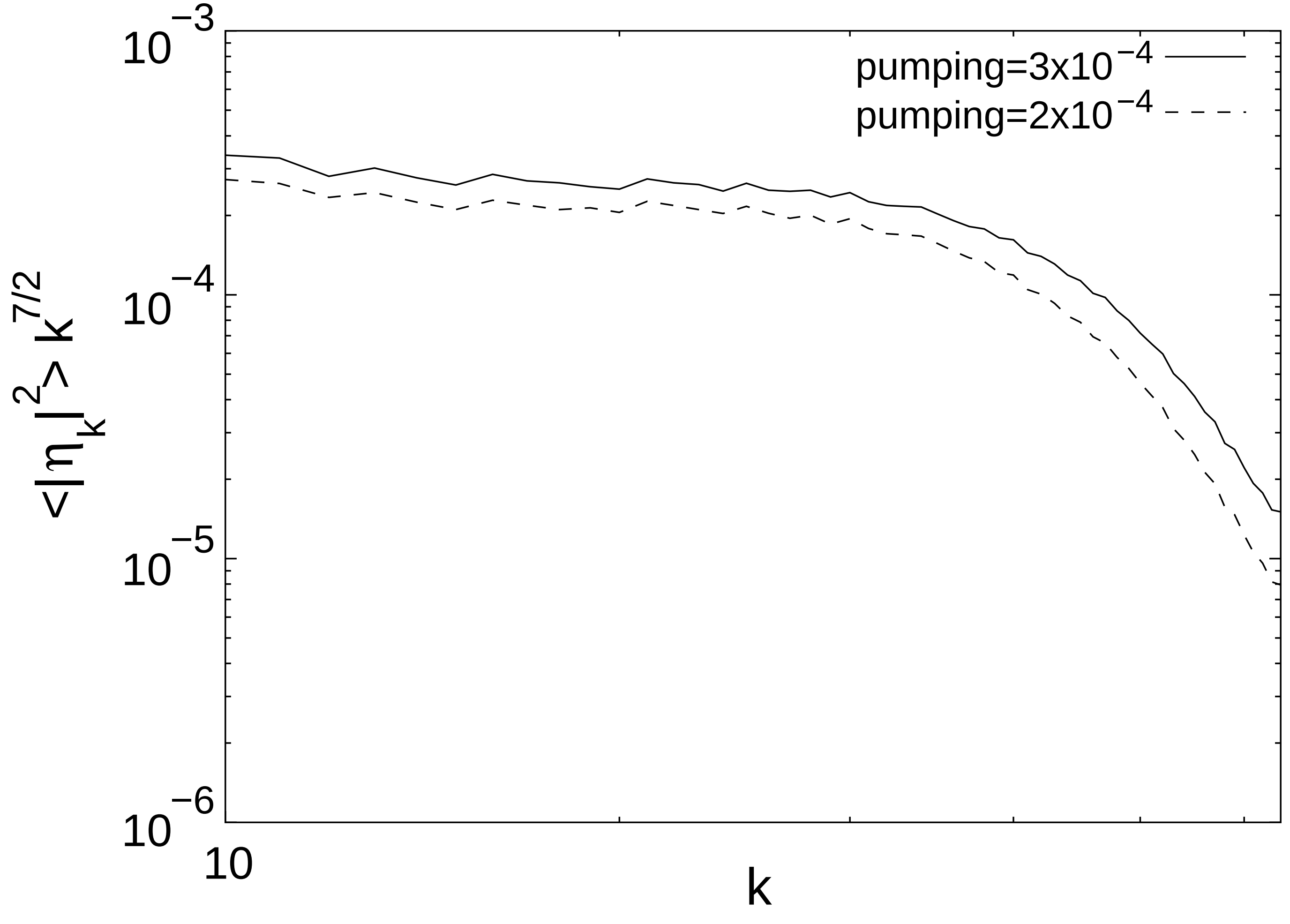

Inverse cascade. Swell simulation. Dynamical equations

We solved the dynamical equations in a box $2\pi \times 2\pi$ by the same spectral code. The number of harmonics was $512 \times 4096 = 2^{21} \simeq 2 \times 10^6$. To figure out a minimal size of corresponding tank, we can assume, that minimal wave-length of a gravitational wave in an absence of capillary effects can be estimated as $\lambda_{min} = 5$ cm. Thus, the minimal equivalent wave tank should be 25×200 m.

Pseudo-viscious damping was chosen as follows

$$\gamma_k = \begin{cases} 0, k < k_d, \\ -\gamma(k - k_d)^2, k \geq k_d, \end{cases} \\ k_d = 1024, \gamma = 5.92 \times 10^3, \tau = 4.22 \times 10^{-4}. \tag{27}$$

Inverse cascade. Initial conditions

As initial condition, we used a Gauss-shaped distribution on a long axis of the wavenumbers plane

$$\begin{cases} |a_{\vec{k}}| = A_i \exp\left(-\frac{1}{2} \frac{\left|\vec{k} - \vec{k}_0\right|^2}{D_i^2} \right), \left|\vec{k} - \vec{k}_0\right| \leq 2D_i, \\ |a_{\vec{k}}| = 10^{-12}, \left|\vec{k} - \vec{k}_0\right| > 2D_i, \end{cases} \tag{28}$$
$$A_i = 0.92 \times 10^{-6}, D_i = 60, \vec{k}_0 = (0; 300), \omega_0 = \sqrt{gk_0}.$$

The initial phases of all the harmonics were random. $g = 1$. The average steepness of this initial condition was $\mu =< |\nabla \eta| >\simeq 0.101$.

Inverse cascade. Initial conditions. $|a_{\vec{k}}|^2$ spectrum

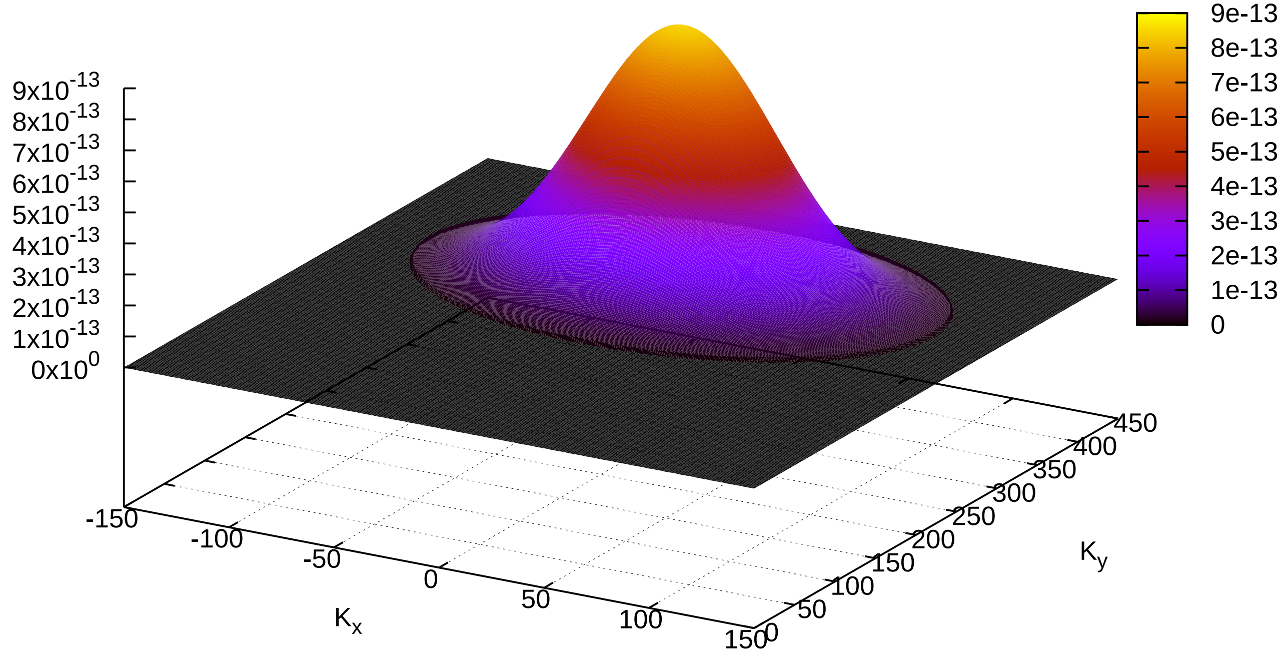

Inverse cascade. Initial conditions. $|a_{\vec{k}}|^2$ spectrum

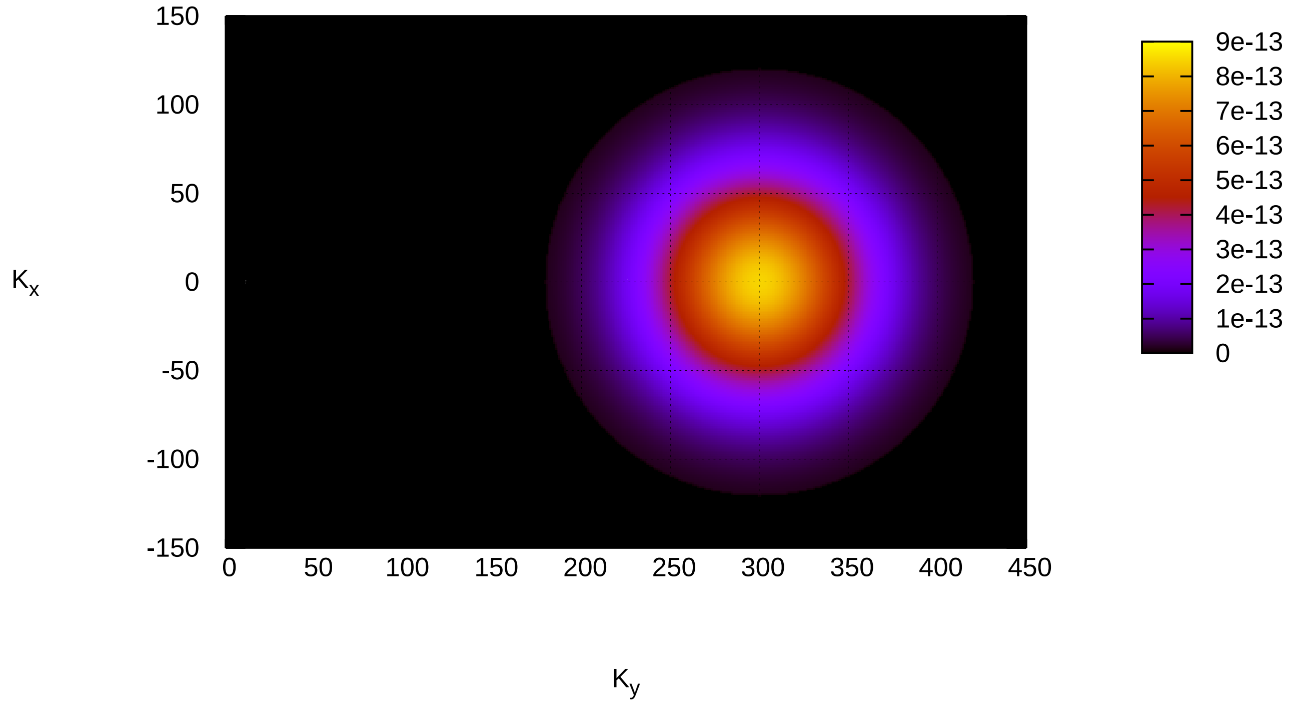

Inverse cascade. Final stage. $|a_{\vec{k}}|^2$ spectrum

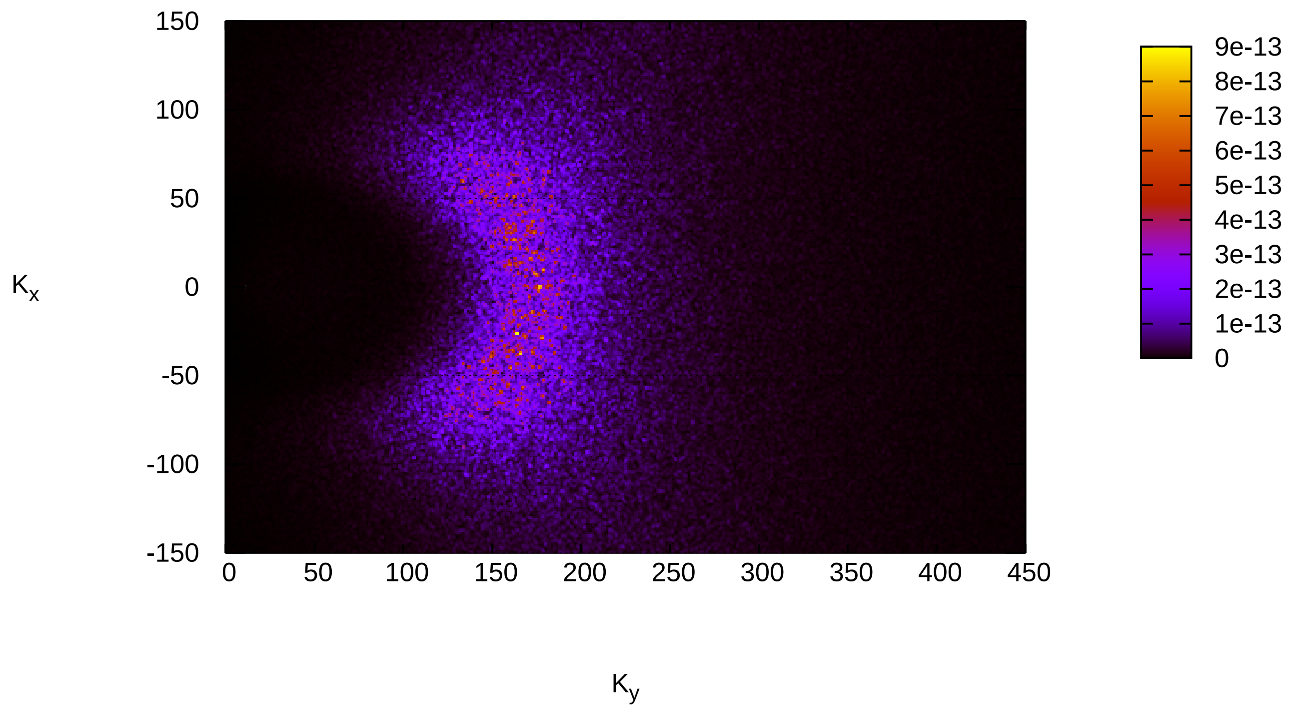

Inverse cascade. Initial conditions. Surface elevation

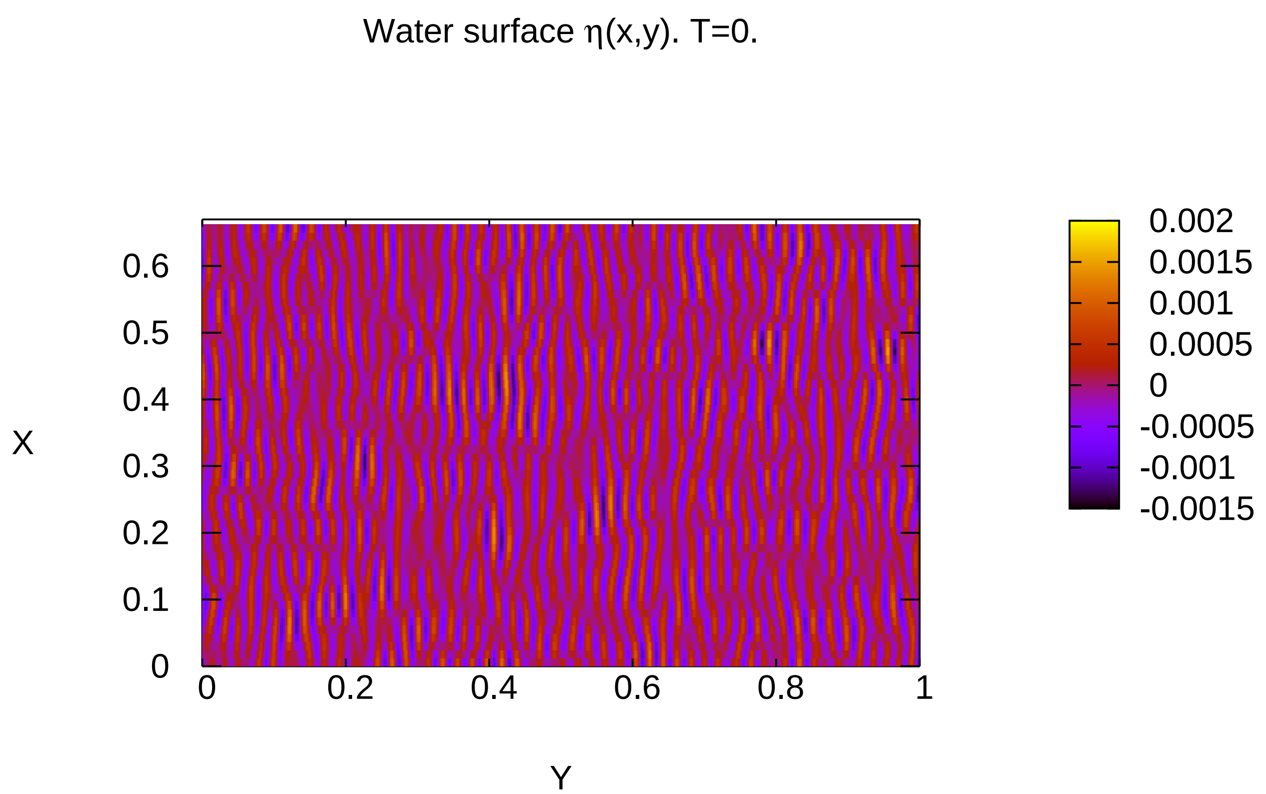

Inverse cascade. Final stage. Surface elevation

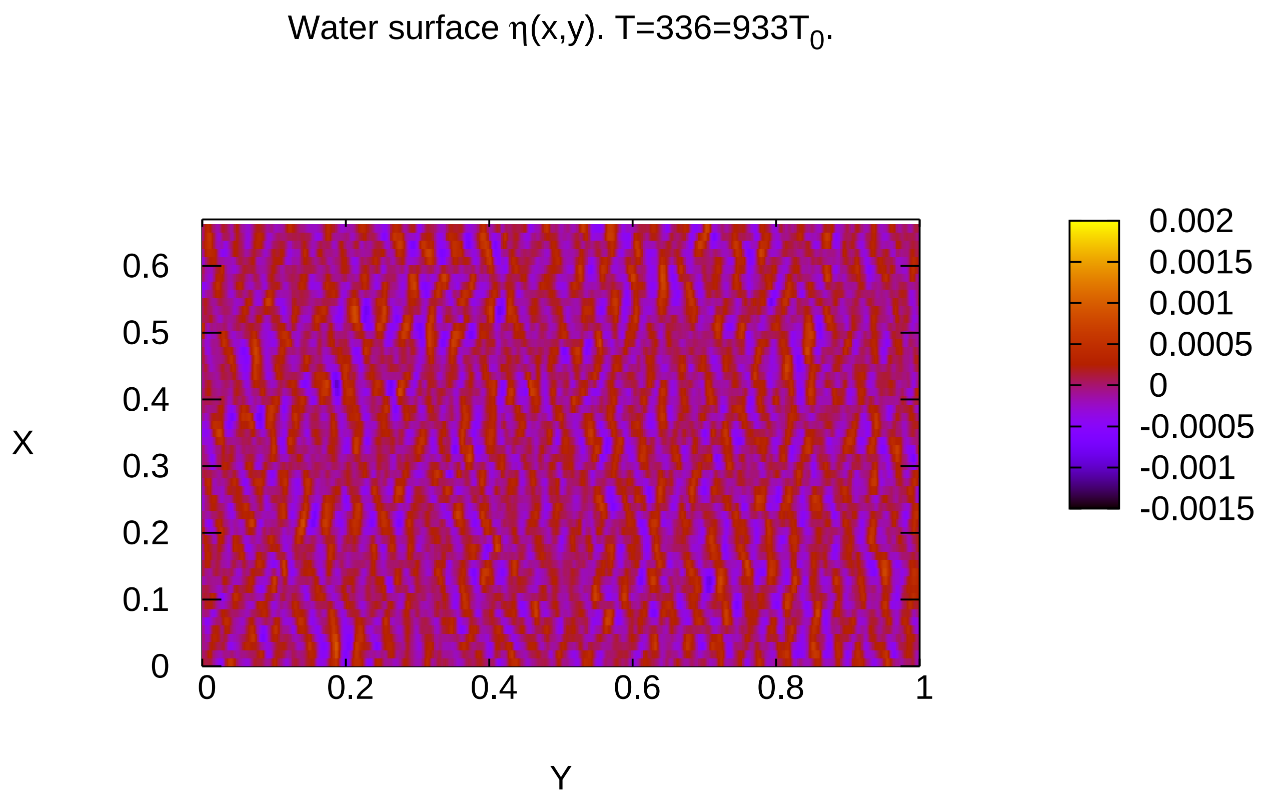

Inverse cascade. Kolmogorov spectrum. ω-space

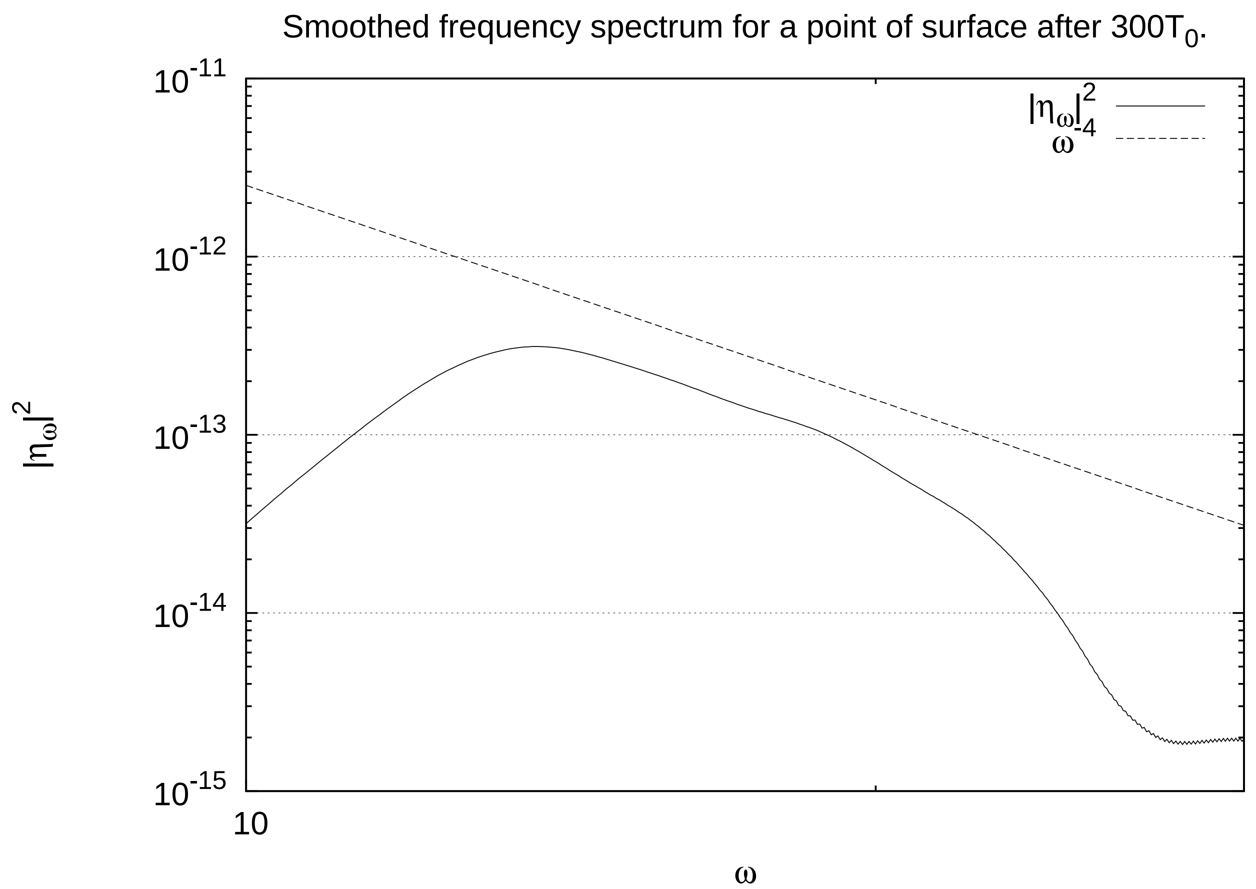

Inverse cascade. Action

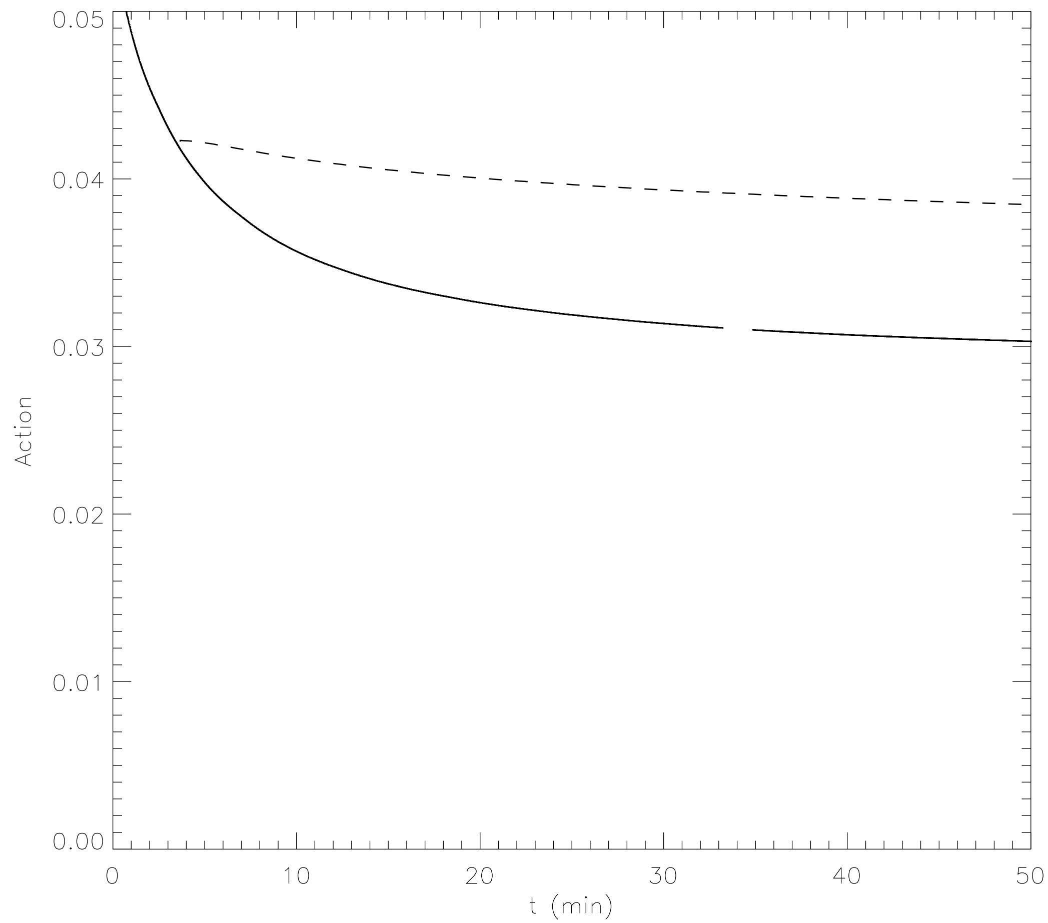

Dashed line – Hasselmann, solid line – dynamical equations

Inverse cascade. PDF of surface elevation

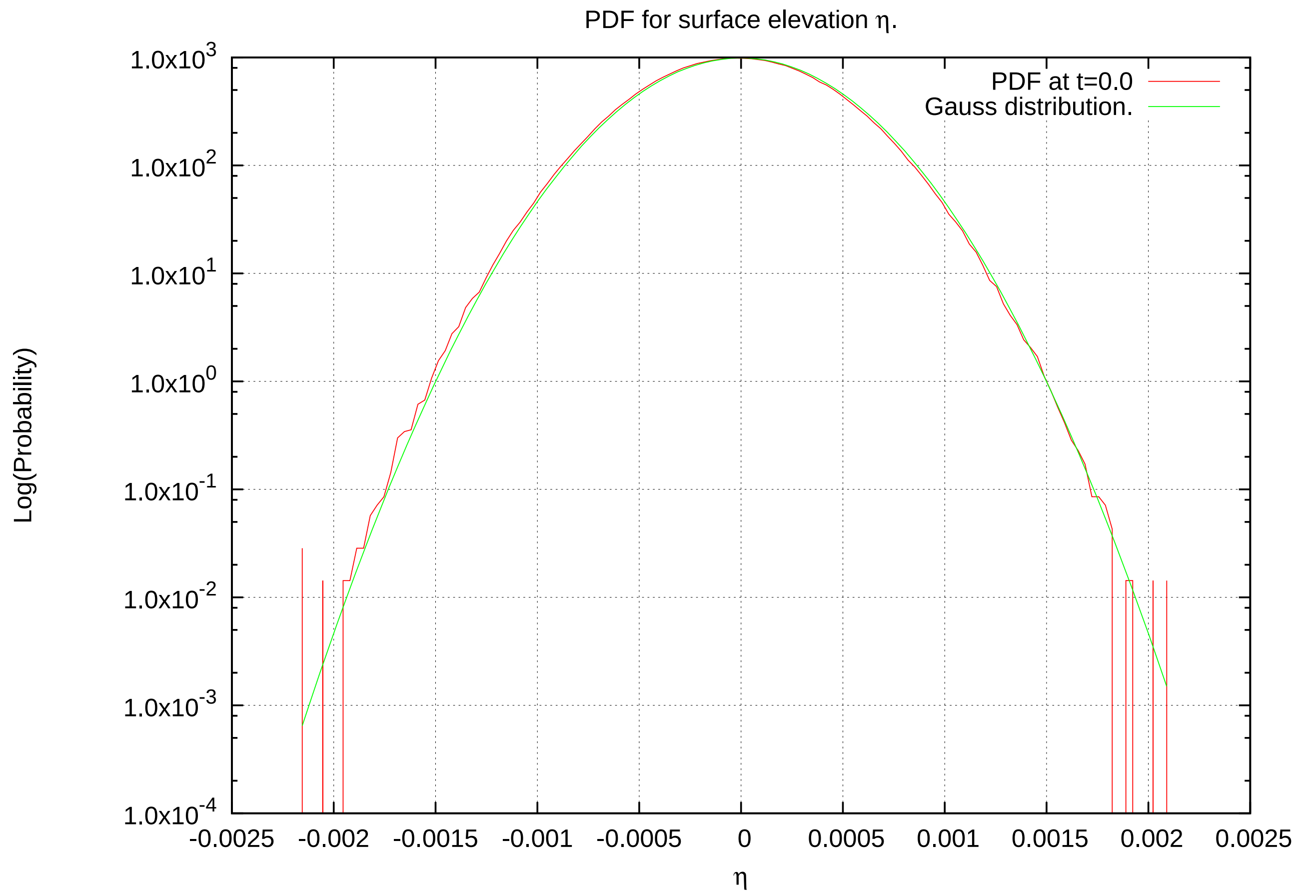

Figure 1: PDF for surface elevation η at initial moment of time. $t = 0$.

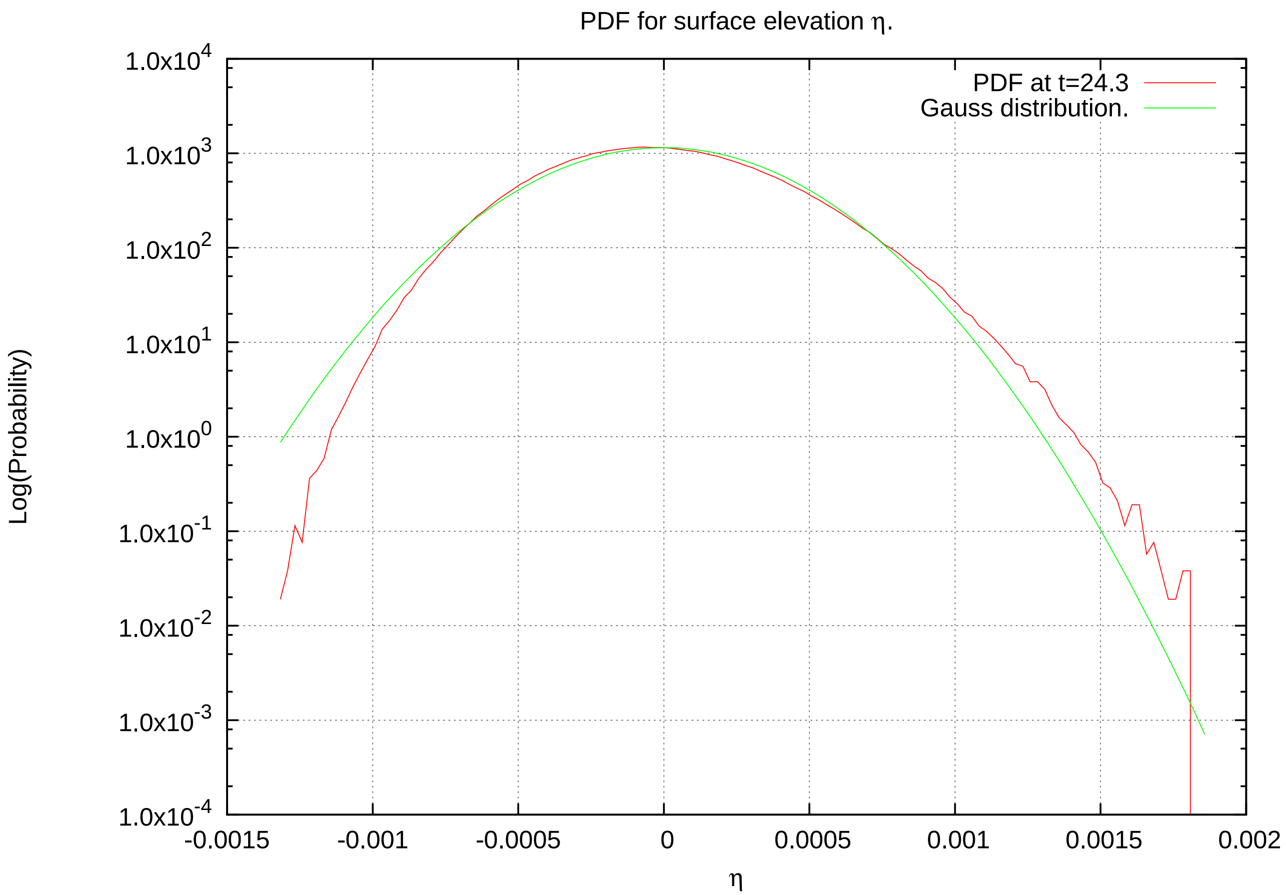

Figure 2: PDF for surface elevation η at sime middle moment of time. $t \simeq 70T_0$.

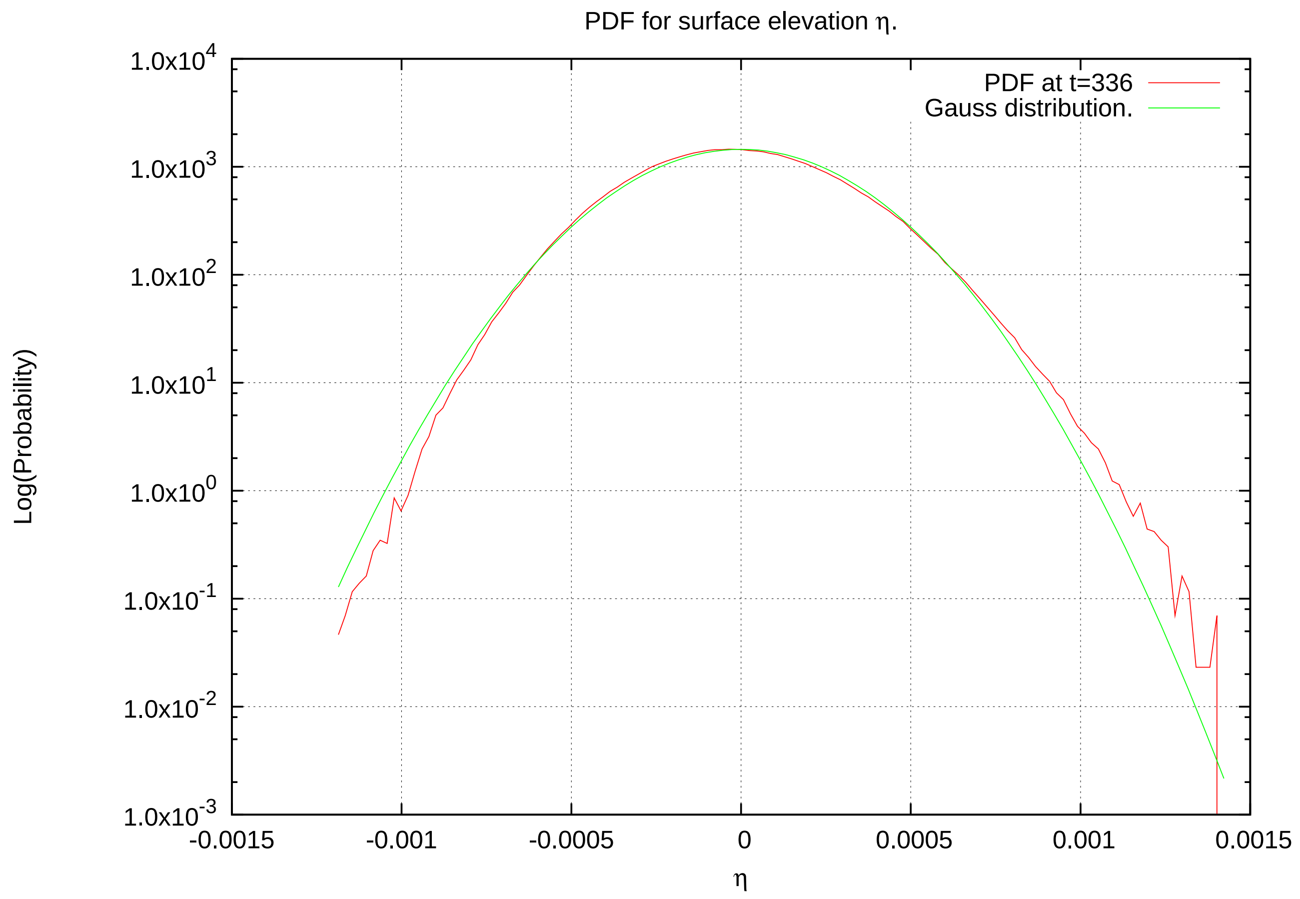

Figure 3: PDF for surface elevation η at final moment of time. $t \simeq 933 T_0$.

Inverse cascade. PDF of surface gradients in longitudinal direction

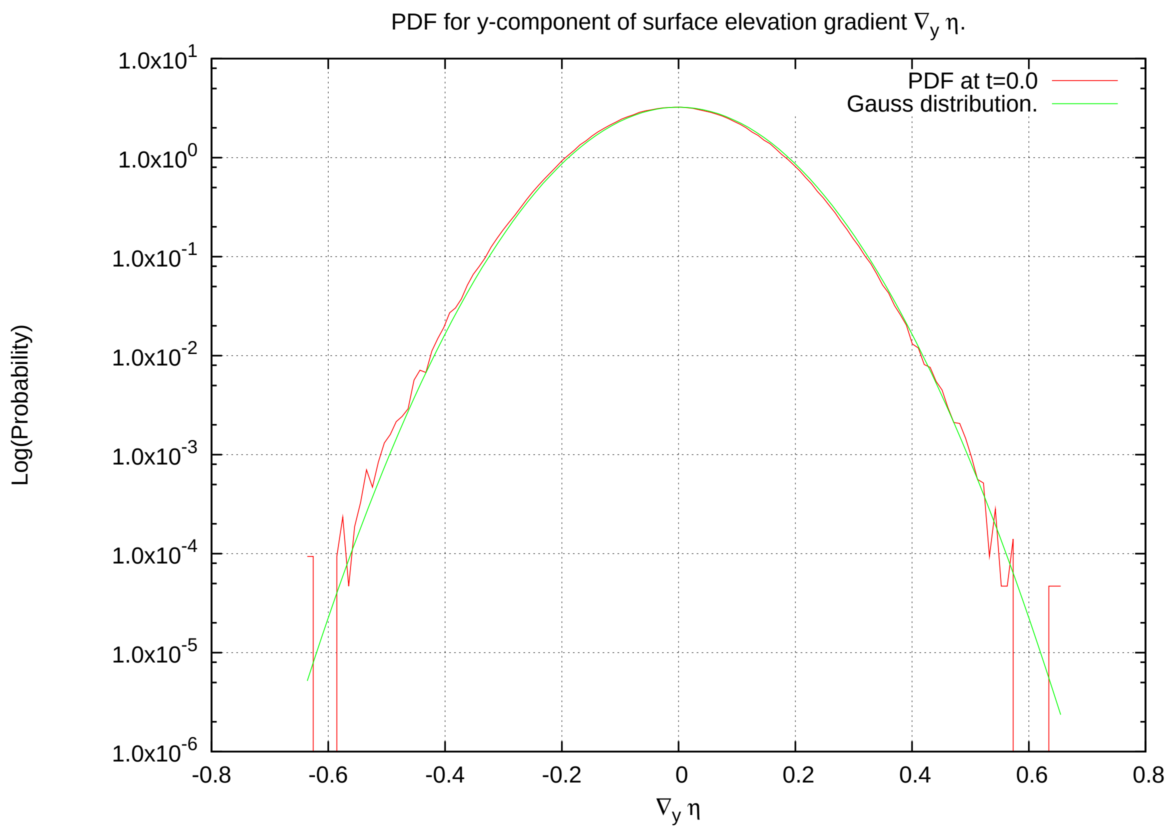

Figure 4: PDF for $(\nabla\eta)_y$ at initial moment of time. $t = 0$.

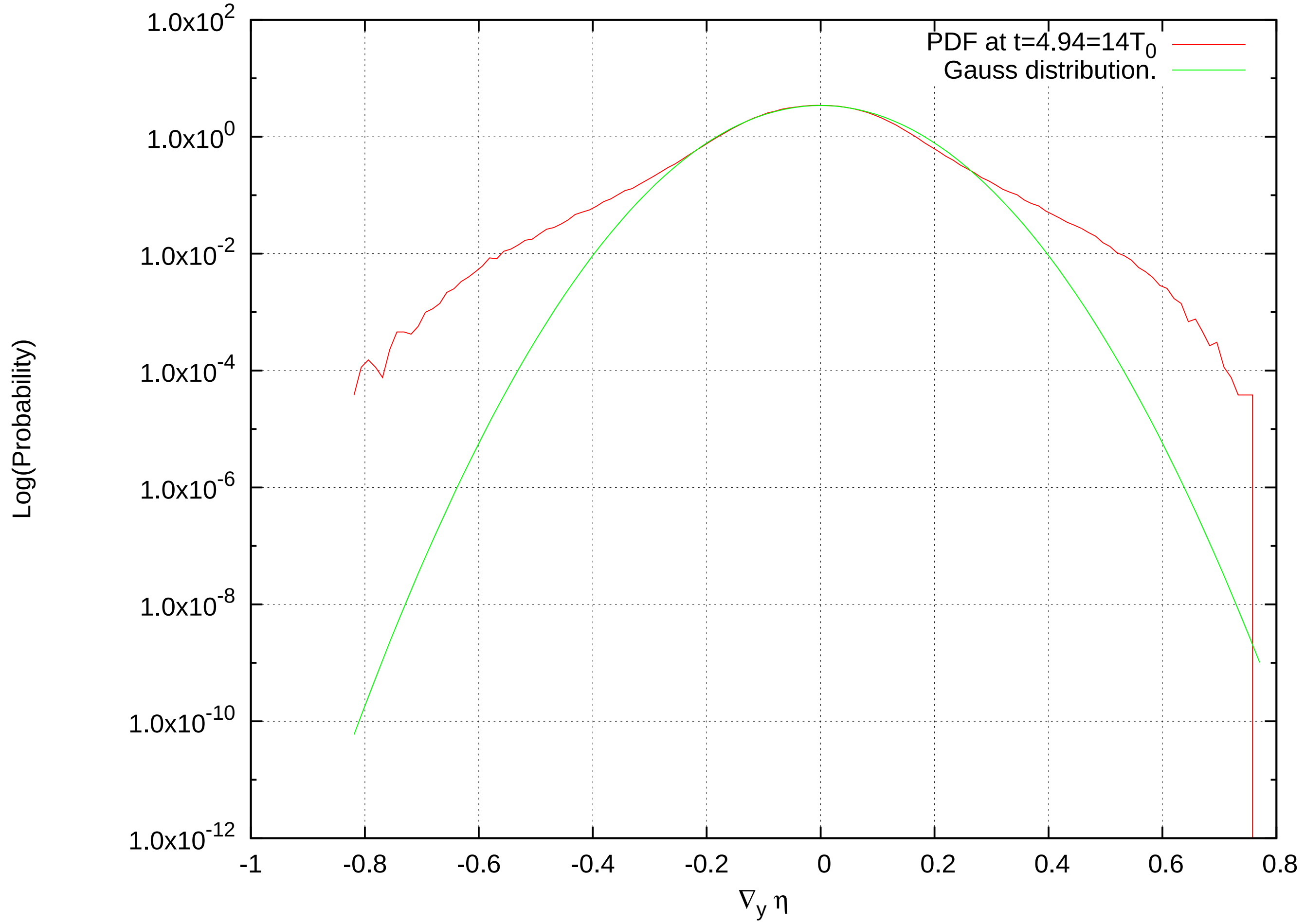

Figure 5: PDF for $(\nabla\eta)_y$ at some middle moment of time. $t \simeq 14T_0$.

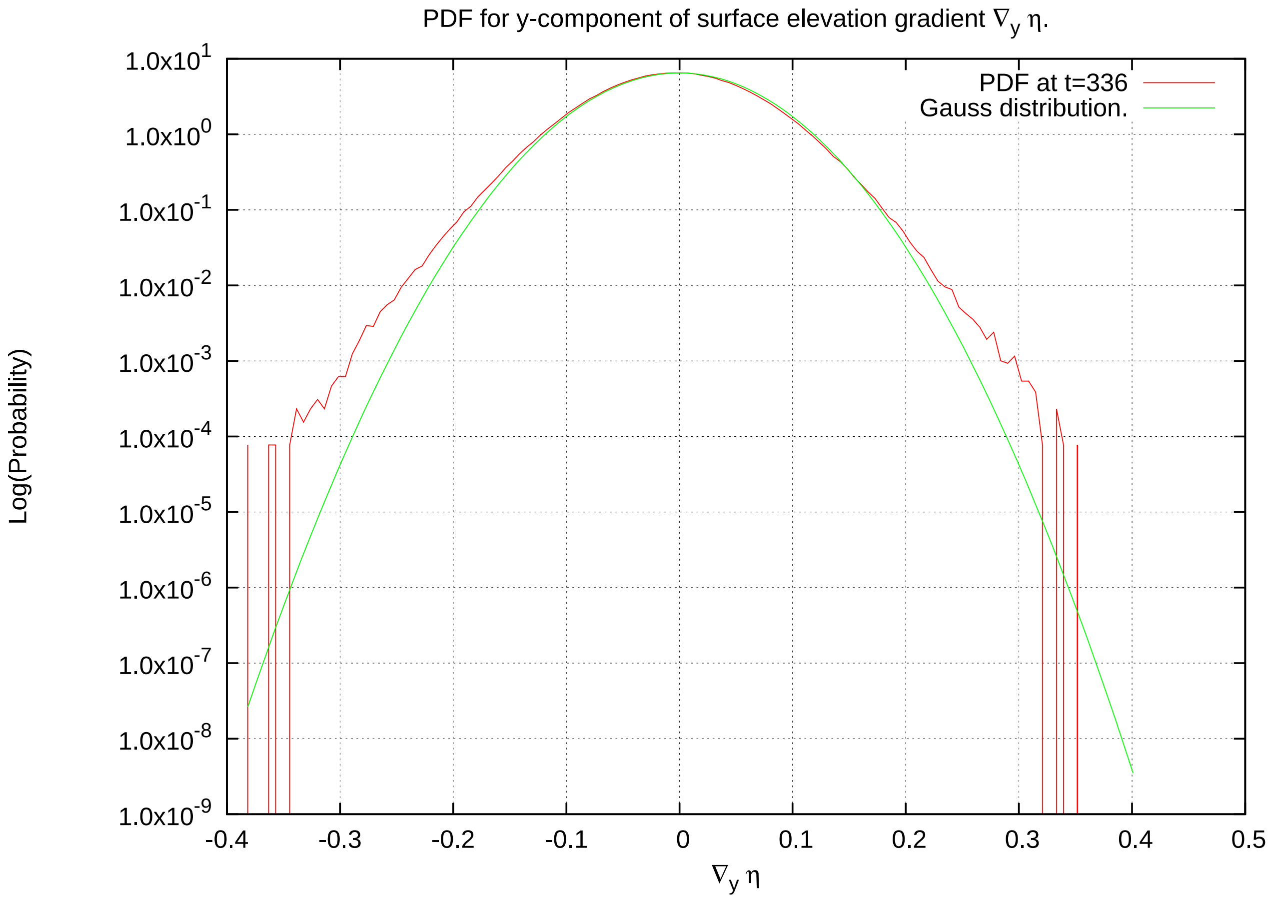

Figure 6: PDF for $(\nabla\eta)_y$ at final moment of time. $t \simeq 933T_0$.

Inverse cascade. Surface elevation at the moment of maximum roughness

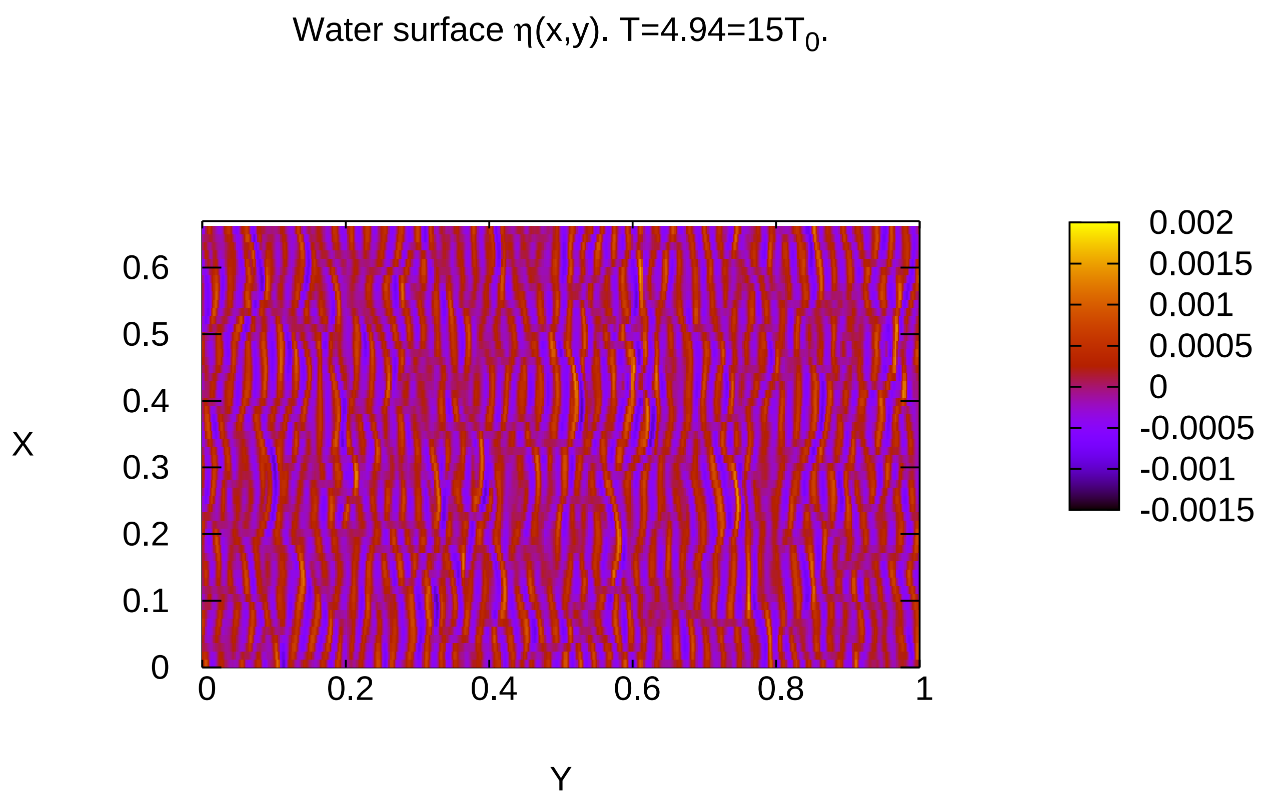

Inverse cascade. Initial conditions. Hasselman equations

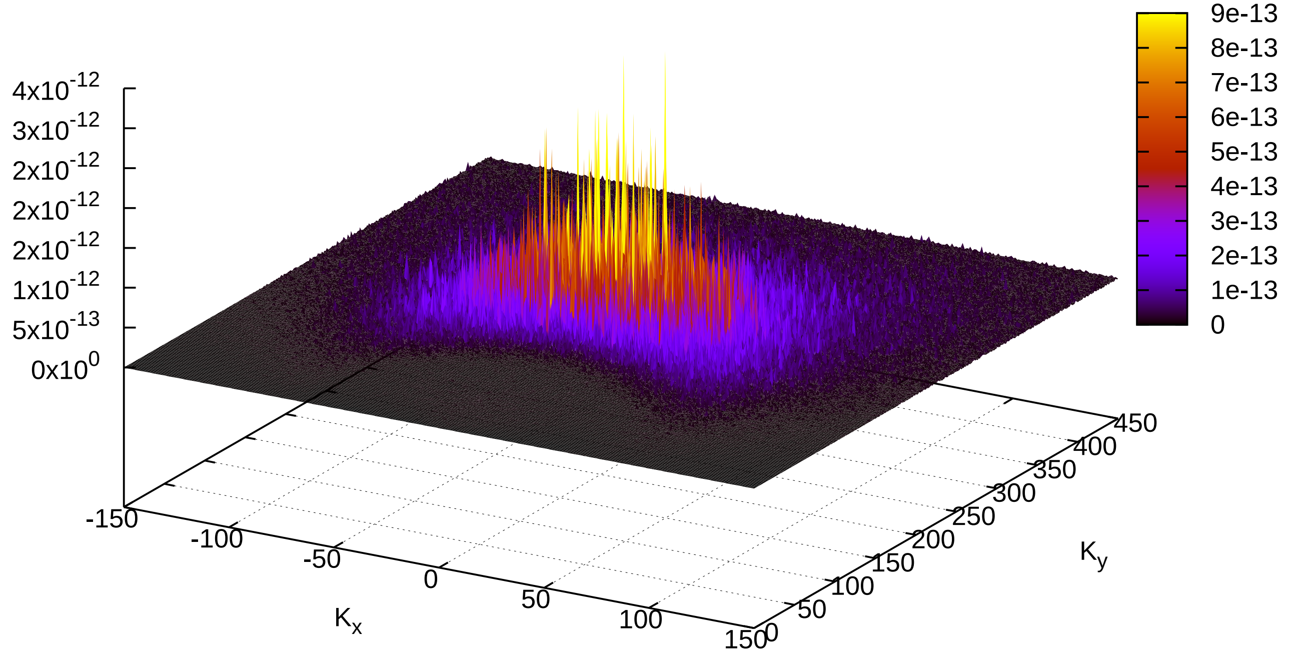

Inverse cascade. Initial conditions. Hasselman equations

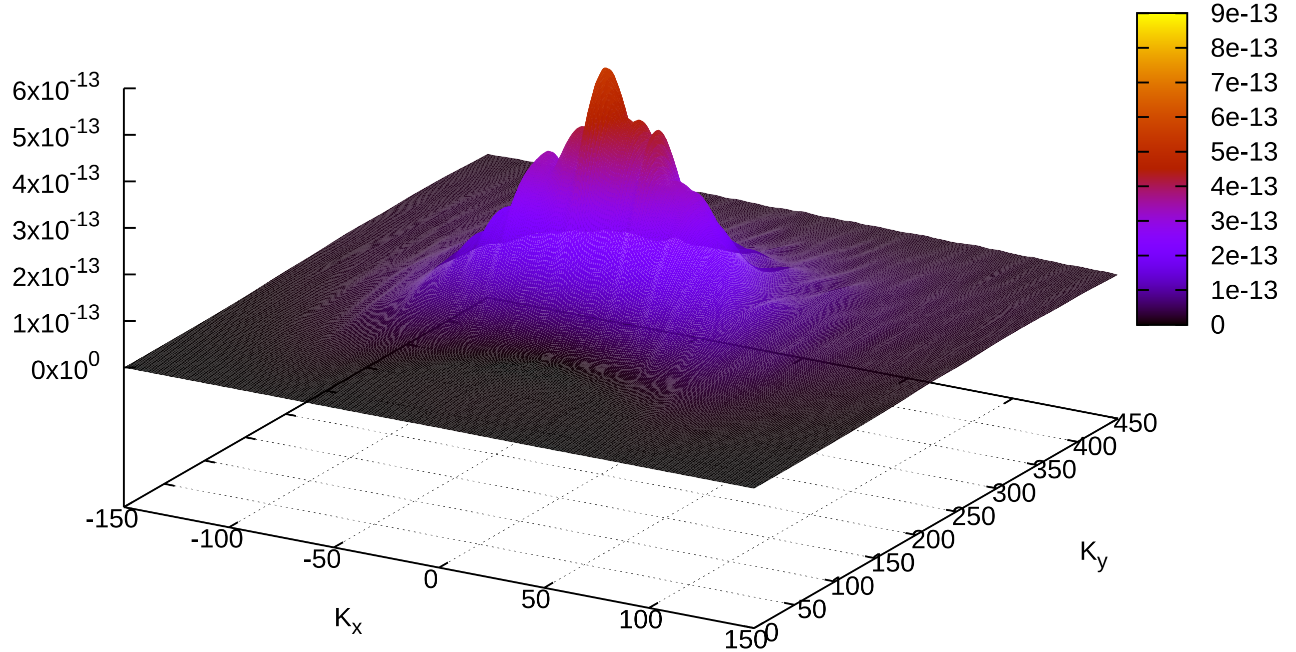

Inverse cascade. Initial conditions. Hasselman equations

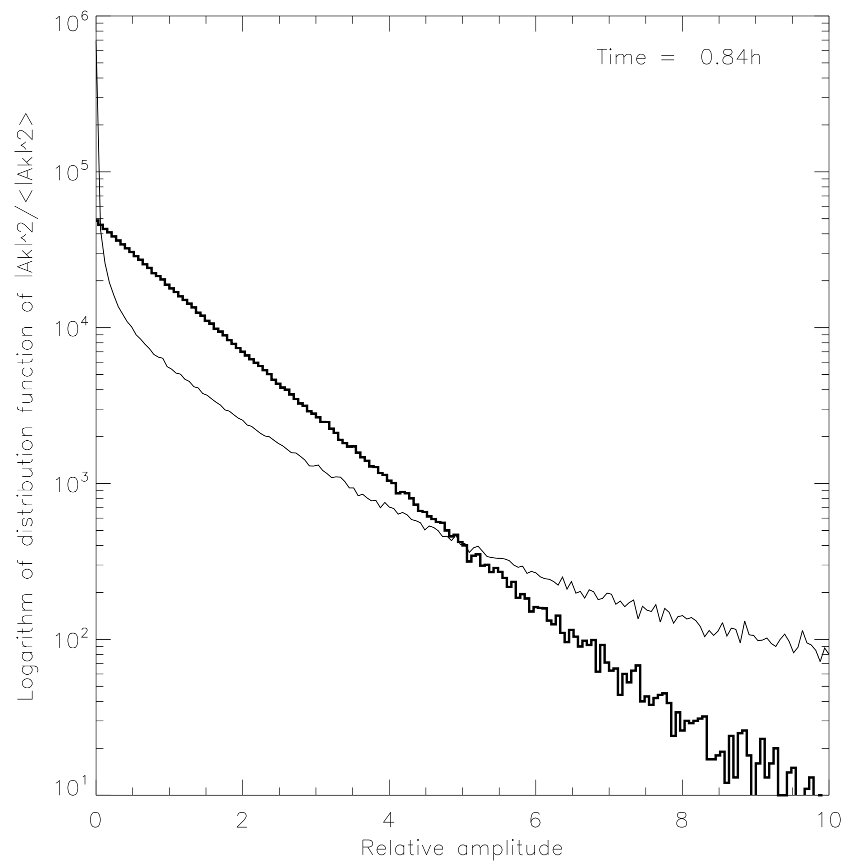

Figure 7: Logarithm of distribution function of $|a_{\vec{k}}|^2/<|a_{\vec{k}}|^2>$.

Inverse cascade. Mesoscopic tubulence

One should remember, that the bold lines in previous figures are results of averaging over a million of harmonics. Among them there is a population of "selected few" or "oligarchs" with amplitude exceeding the average value more than ten times. The "oligarchs" do exist because our grid is still not fine enough. The resonant conditions

$$\begin{aligned} \omega_k + \omega_{k_1} = \omega_{k_2} + \omega_{k_3}, \\ \vec{k} + \vec{k}_1 = \vec{k}_2 + \vec{k}_3, \end{aligned} \qquad (29)$$

give us five-dimensional hypersurface in six-dimensional space $\vec{k}, \vec{k}_1, \vec{k}_2$. In any finite system, (29) turns to Diophantine equation. However in reality energy transport is realized not by exact, but by "approximate" resonances, posed in a layer near the resonant surface and defined by condition

$$|\omega_k + \omega_{k_1} - \omega_{k_2} - \omega_{k+k_1-k_2}| < \gamma, \qquad (30)$$

here γ — is a characteristic inverse time of nonlinear interaction.

In a finite system $\vec{k}, \vec{k}_1, \vec{k}_2$ take values in nodes of the discrete grid. The weak turbulent approach is valid, if the density of discrete approximate resonanses inside the layer (30) is high. In our case the lattice constant $\Delta k = 1$, and typical relative deviation from the resonance surface

$$\frac{\Delta\omega}{\omega} \simeq \frac{\omega'_k}{\omega}\Delta k = \frac{\omega'_k}{\omega} \simeq \frac{1}{600} \simeq 2 \times 10^{-3}. \tag{31}$$

Inverse time of interaction γ can be estimated from our numerical experiments: wave amplitudes change essentially during 30 periods, and one can assume: $\gamma/\omega \simeq 10^{-2} \gg \frac{\delta\omega}{\omega}$. It means that the condition for the applicability of weak turbulent theory is typically satisfied but the "reserve" for the validity is rather modest. As a result some particular harmonics, posed in certain "privileged" point of k-plane could form a "network" of almost resonant quadruplets and realize significant part of energy transport. Amplitudes of these harmonics exceed the average level essentially. This effect was described in the previous article, where such "selected few" harmonics were called "oligarchs". If "oligarchs" realize most part of energy flux, the turbulence is "mesoscopic", not weak.

In our case "oligarchs" do exist, but their contribution in the total wave action is not more 4%.

Inverse cascade. Instant spectrum snapshot. Dynamical equations

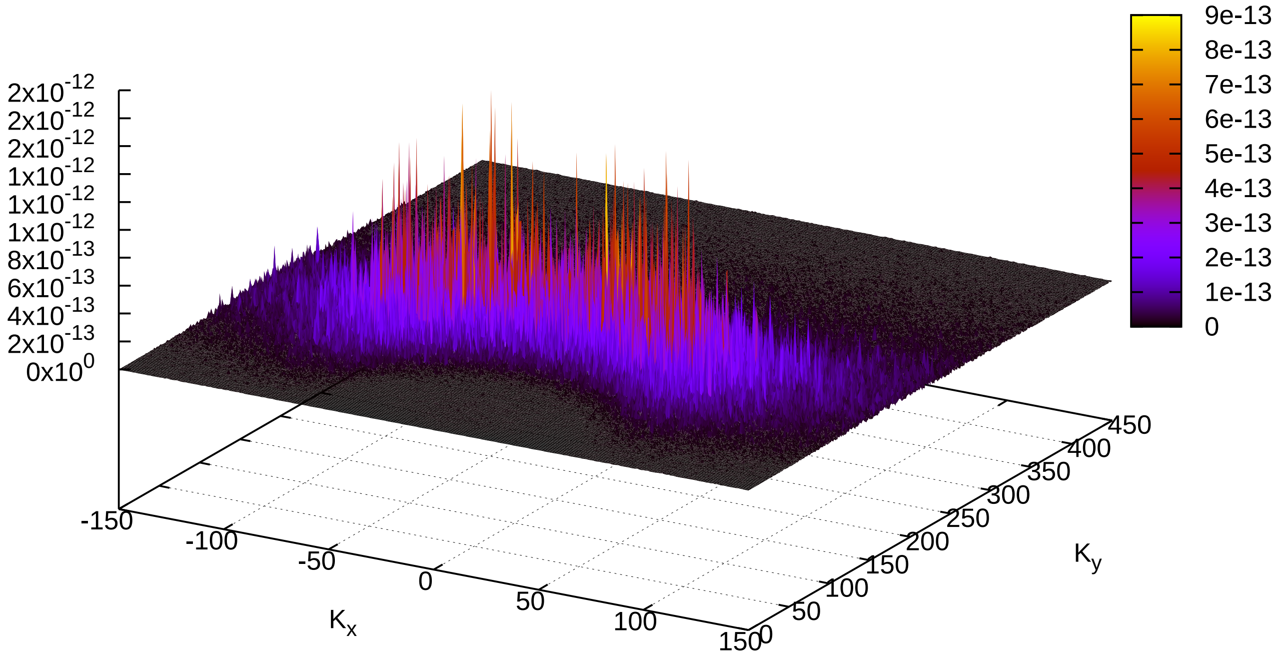

Inverse cascade. Spectrum averaged over 244 periods. Dynamical equations

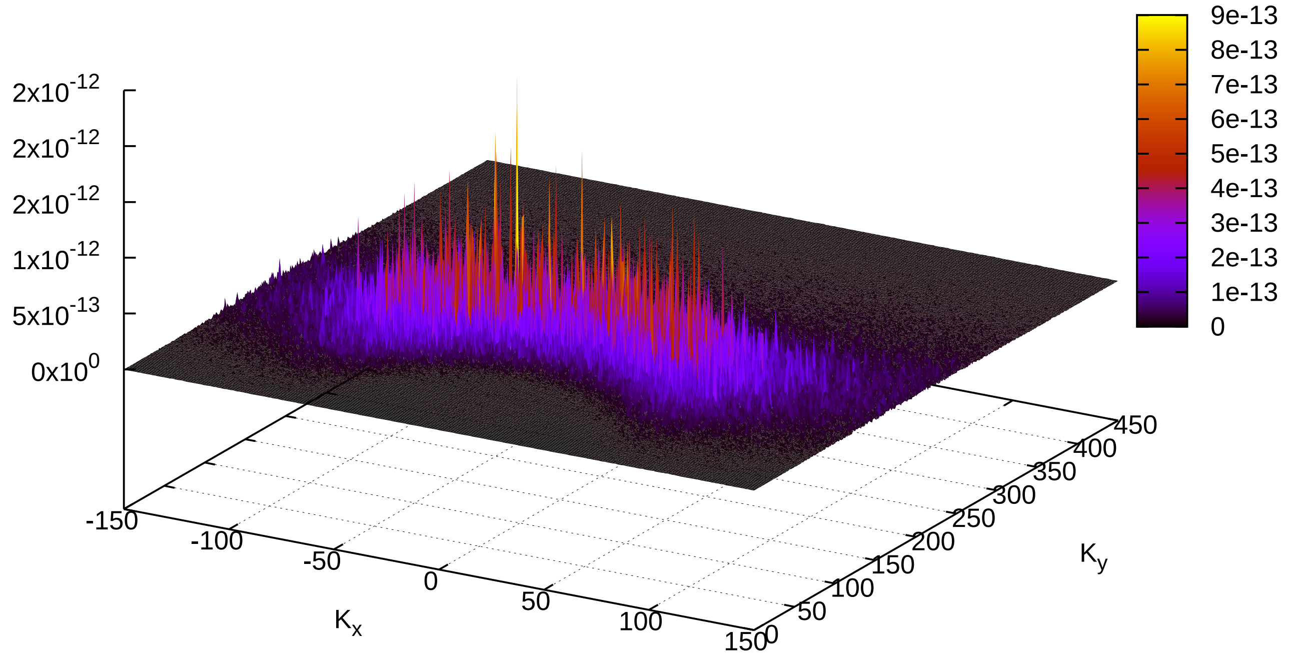

From dynamical equations to Hasselmann equation.

Standard setup for numerical simulation of the dynamical equations, implies $2\pi\times 2\pi$ domain in real space and gravity acceleration $g = 1$. Usage of the dimension of 2π is convenient because in this case wavenumbers are integers.

In the contrary to dynamical equations, the kinetic equation solution algorithm is formulated in terms of real physical variables and it is necessary to describe the transformation from the “dynamical” variables into to the “physical” ones.

Scaling from “dynamical” to “real” variables is the following:

$$\eta_{\vec{r}} = \alpha\eta'_{\vec{r}'}, \quad \vec{k} = \frac{1}{\alpha}\vec{k}', \quad \vec{r} = \alpha\vec{r}', \quad g = \nu g', \tag{32}$$

$$t = \sqrt{\frac{\alpha}{\nu}}t', \quad L_x = \alpha L'_x, \quad L_y = \alpha L'_y \tag{33}$$

where prime denotes variables corresponding to dynamical equations.

In current simulation we used stretching coefficient $\alpha = 800.00$, which allows to define physical dimensions of the discussed simulation: we considered $5026m \times 5026m$ ocean domain with characteristic wavelength of the initial condition around $22m$.

Inverse cascade. Comparison of deterministic and statistical experiments.

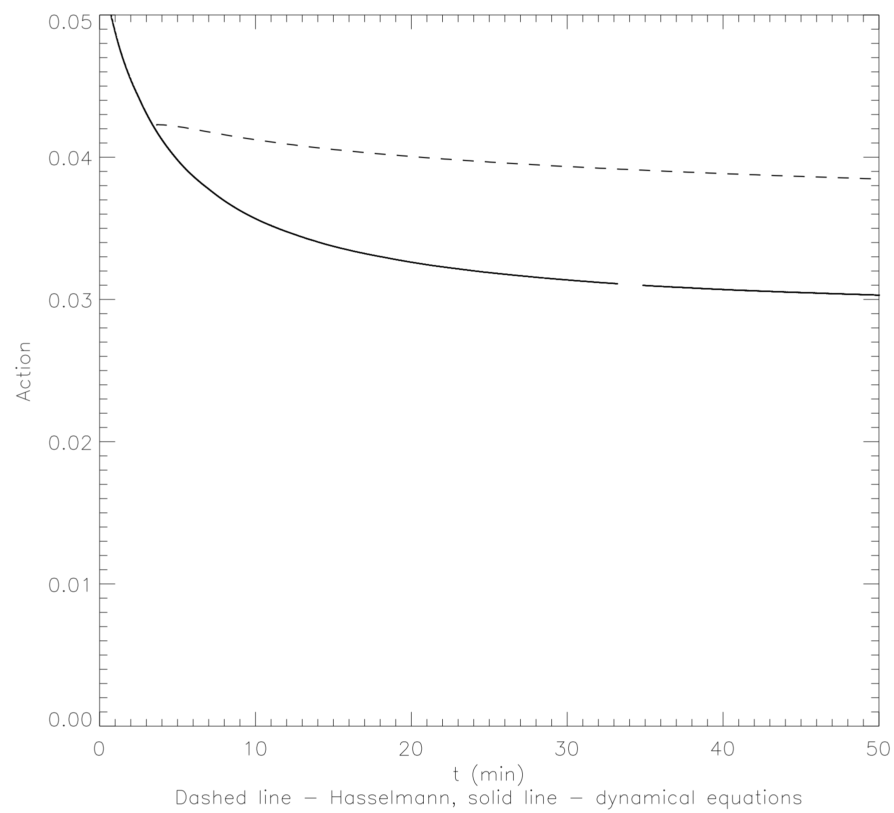

Figure 8: Total wave action as a function of time for artificial viscosity case

Numerical Verification of the Hasselmann equation.

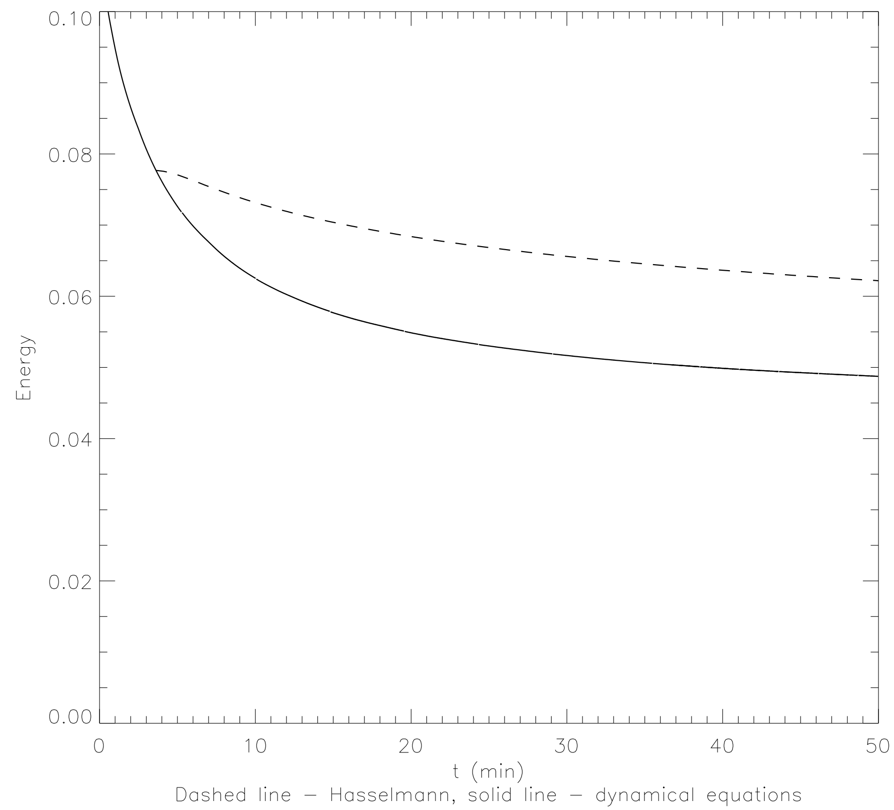

Figure 9: Total wave energy as a function of time for artificial viscosity case

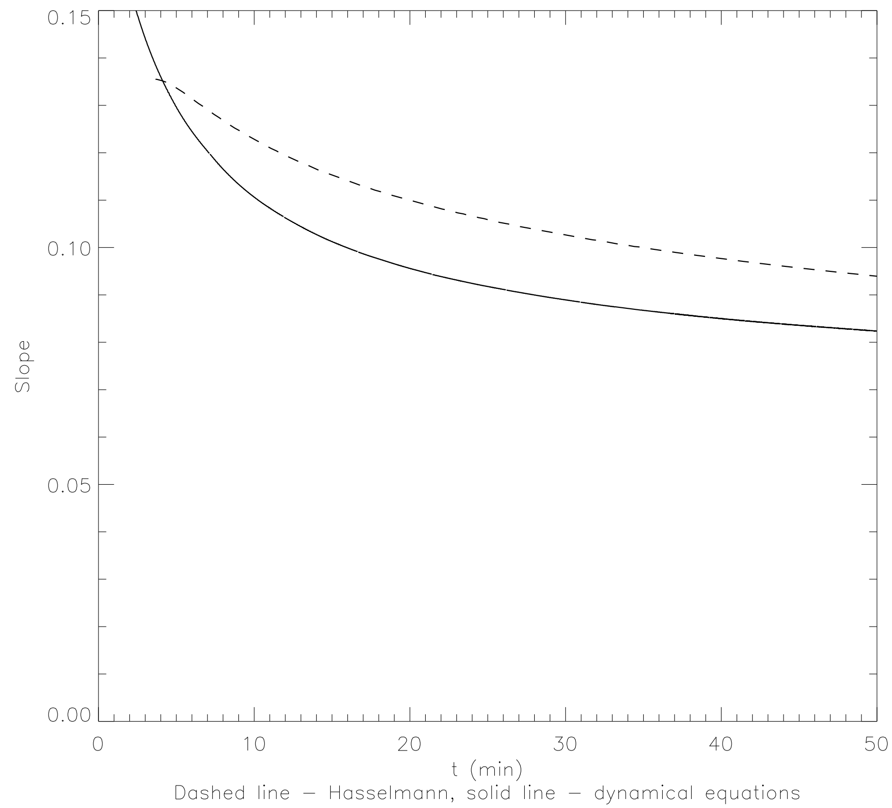

Figure 10: Average waves slope as a function of time for artificial viscosity case

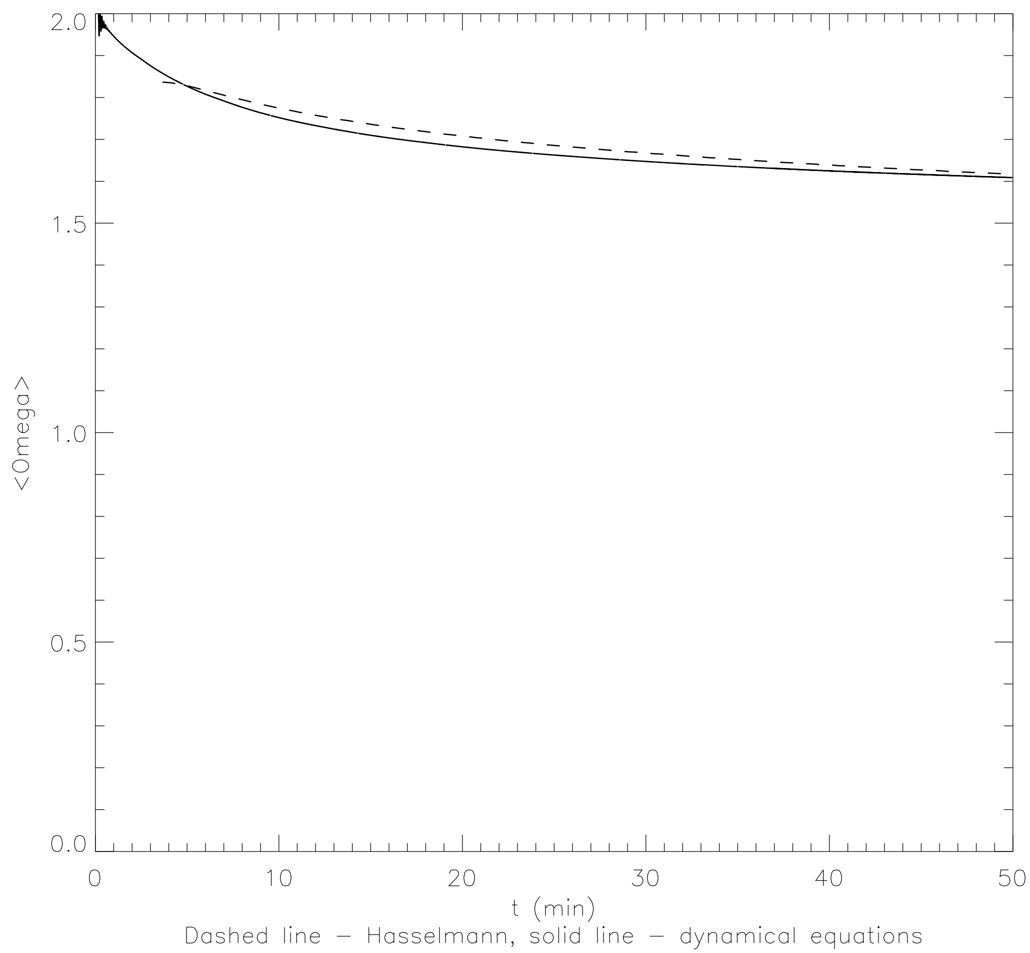

Figure 11: Mean wave frequency as a function of time for artificial viscosity case.

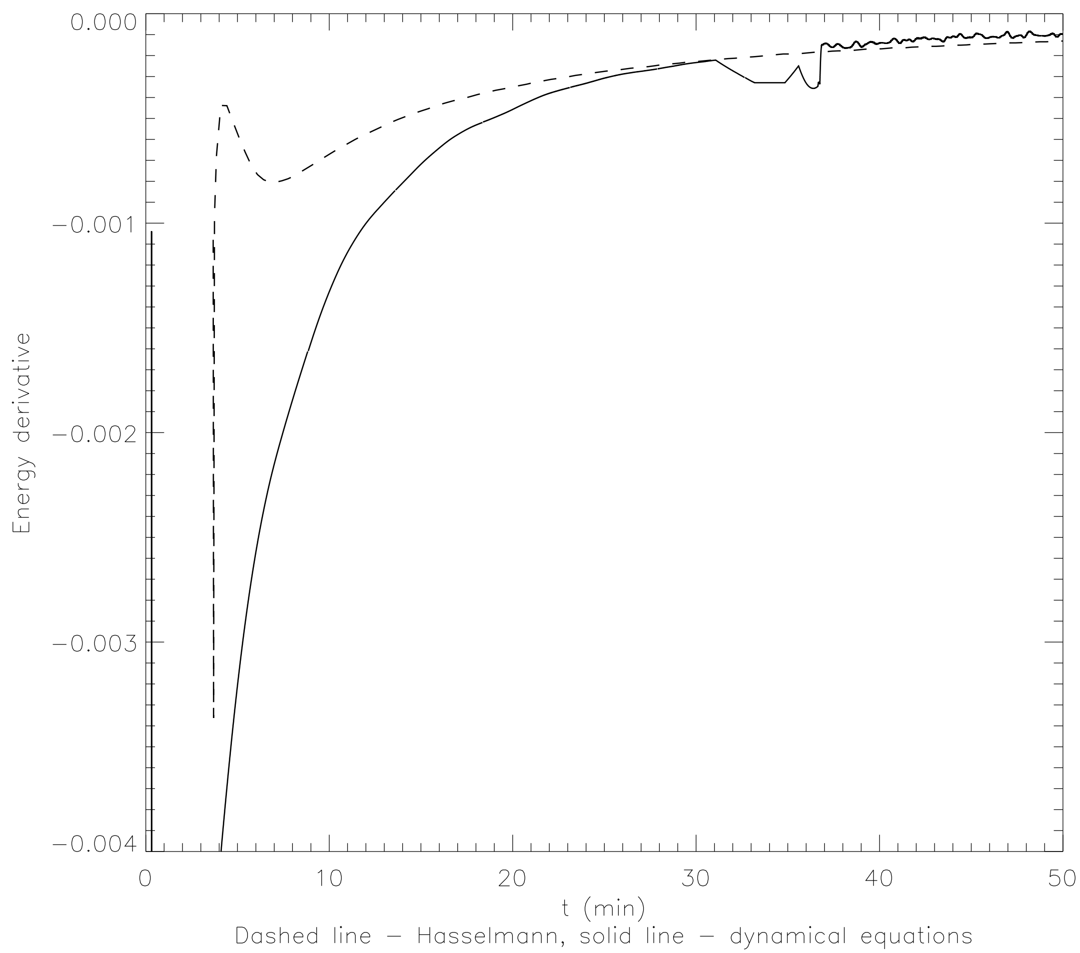

Figure 12: Total wave energy time derivative as a function of time for artificial viscosity case.

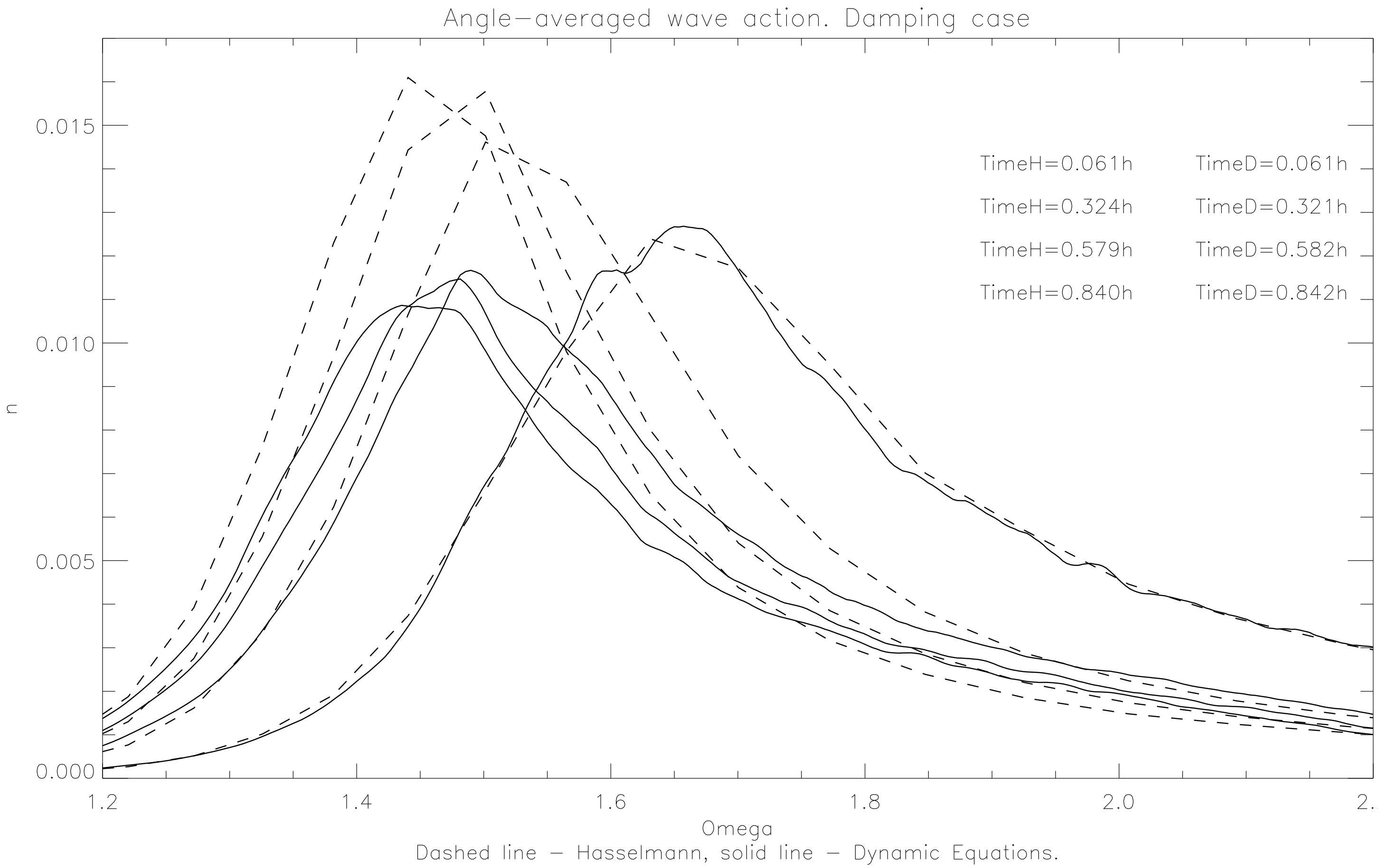

Figure 13: Angle-averaged spectrum as a function of time for dynamical and Hasselmann equations for artificial viscosity case.

Inverse cascade. WAM1 and WAM2 dissipation terms in Hasselmann equation.

Viscous terms referred as $WAM1$ and $WAM2$ are "white-capping" terms, describing energy dissipation by surface waves due to wave breakings, as used in $SWAN$ and WAM wave forecasting models:

$$\gamma_{\vec{k}} = C_{ds}\tilde{\omega}\frac{k}{\tilde{k}}\left((1-\delta)+\delta\frac{k}{\tilde{k}}\right)\left(\frac{\tilde{S}}{\tilde{S}_{pm}}\right)^{p} \tag{34}$$

where k and ω are wave number and frequency, tilde denotes mean value; C_{ds}, δ and p are tunable coefficients; $S = \tilde{k}\sqrt{H}$ is the overall steepness; $\tilde{S}_{PM} = (3.02\times 10^{-3})^{1/2}$ is the value of $\tilde{S}$ for the Pierson-Moscowitz spectrum (note that the characteristic steepness $\mu = \sqrt{2}S$).

Values of tunable coefficients for $WAM1$ case (corresponding to *WAM cycle 3* dissipation) are:

$$C_{ds} = 2.36 \times 10^{-5}, \;\; \delta = 0, \;\; p = 4. \tag{35}$$

Values of tunable coefficients for $WAM2$ case (corresponding to *WAM cycle 4* dissipation) are:

$$C_{ds} = 4.310 \times 10^{-5}, \;\; \delta = 0.5, \;\; p = 4. \tag{36}$$

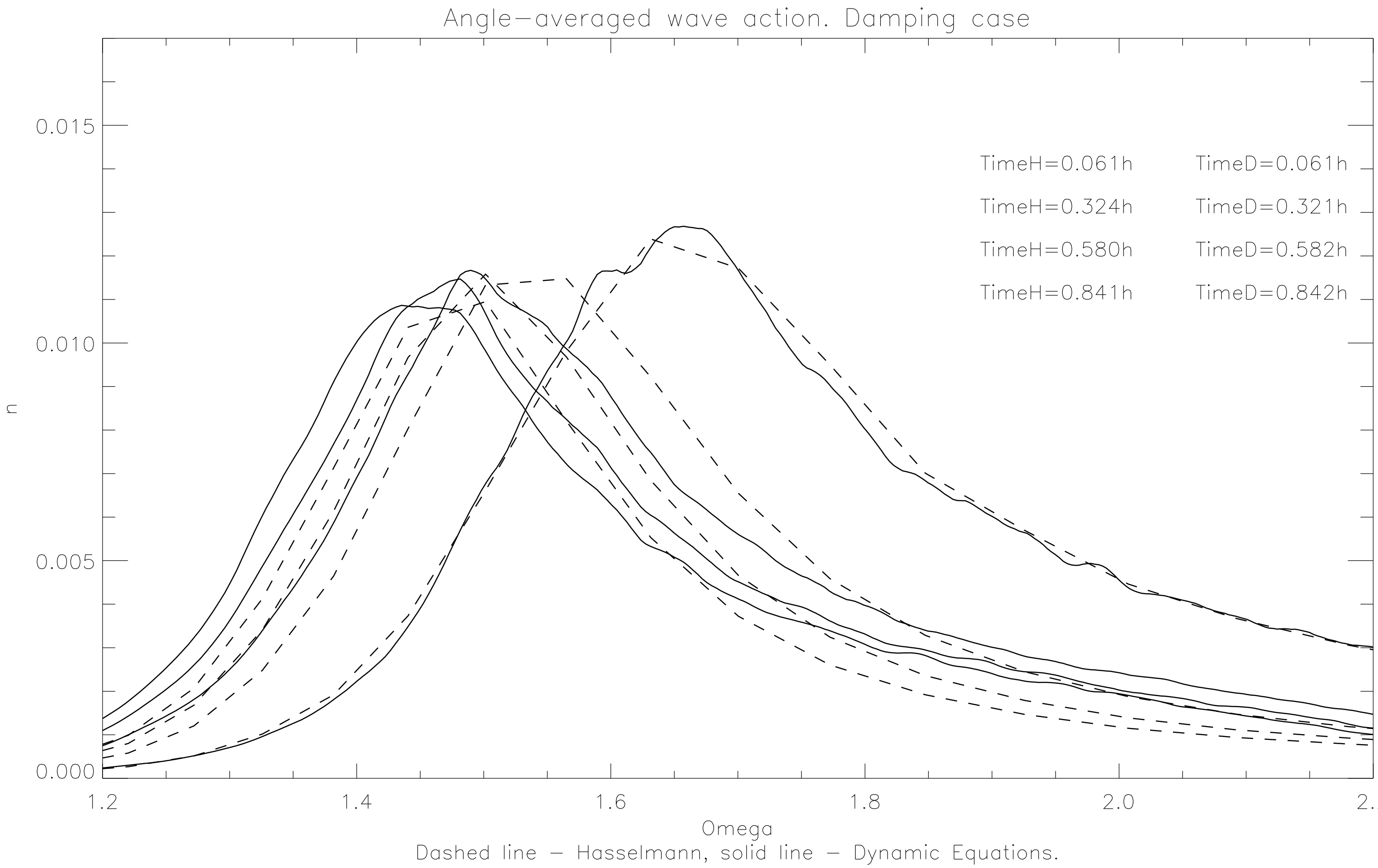

Figure 14: Angle-averaged spectrum as a function of time for dynamical and Hasselmann equations a function of time for WAM1 case.

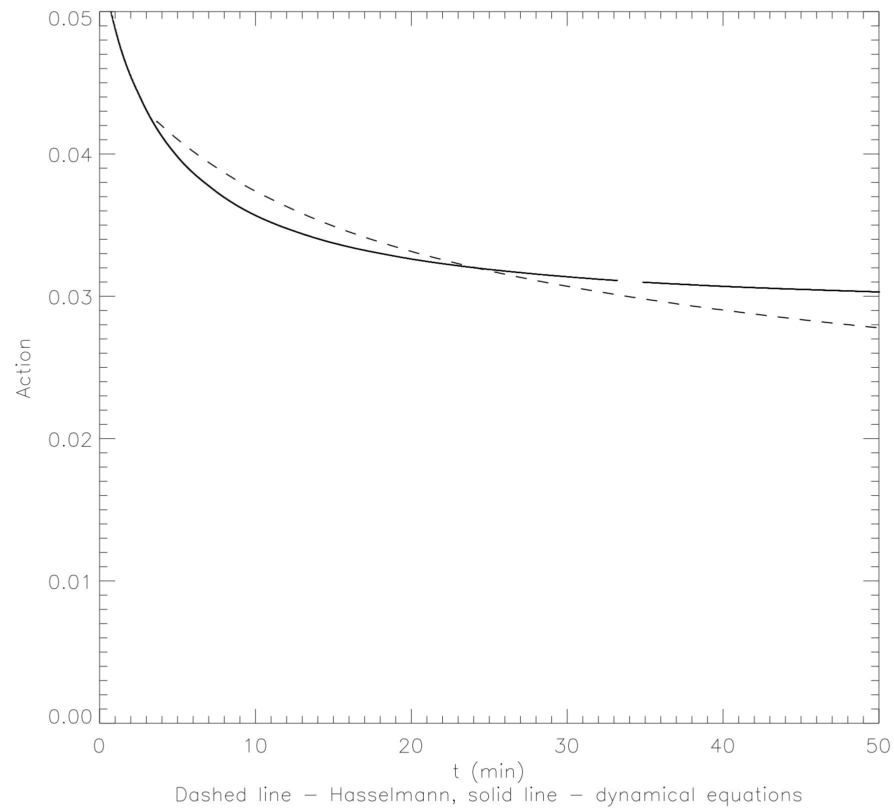

Figure 15: Total action as a function of time for $WAM1$ case

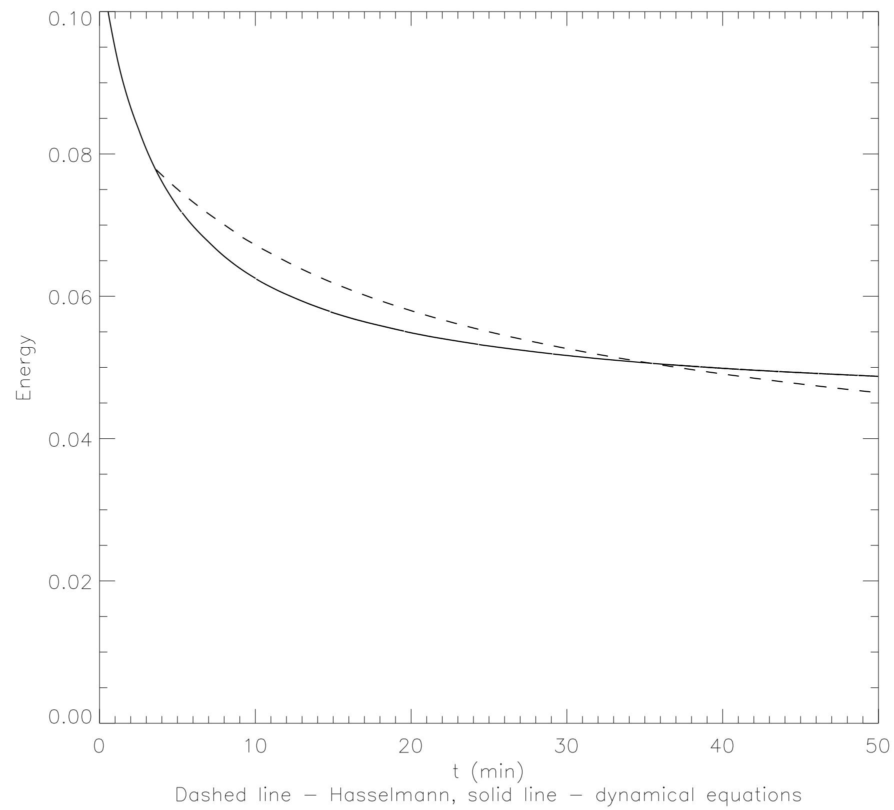

Figure 16: Total wave energy as a function of time for $WAM1$ case

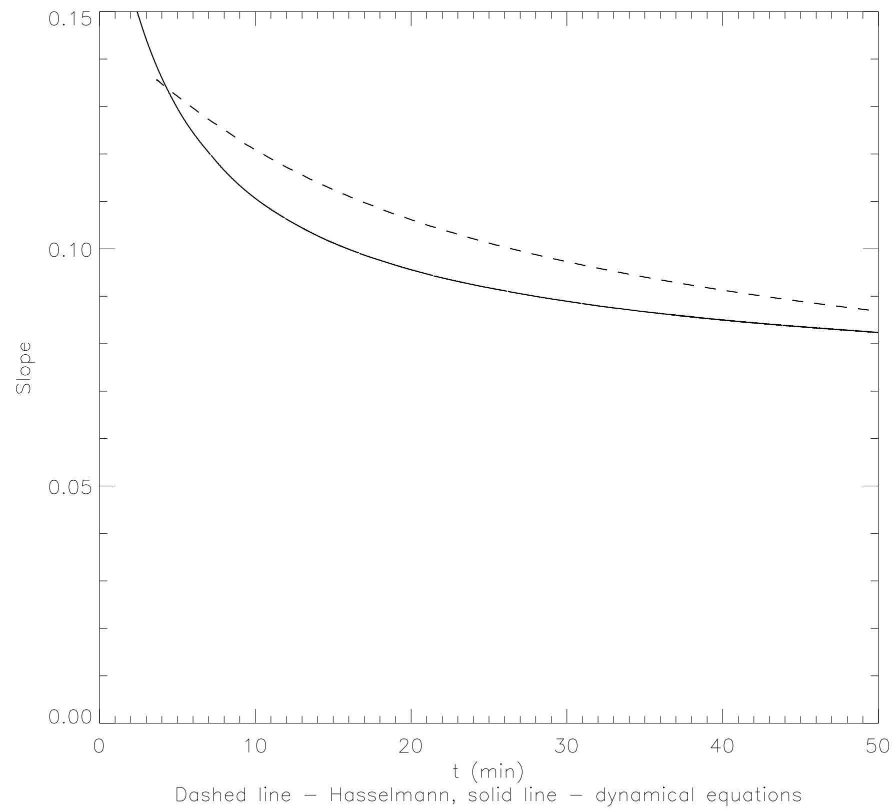

Figure 17: Average waves slope as a function of time for $WAM1$ case

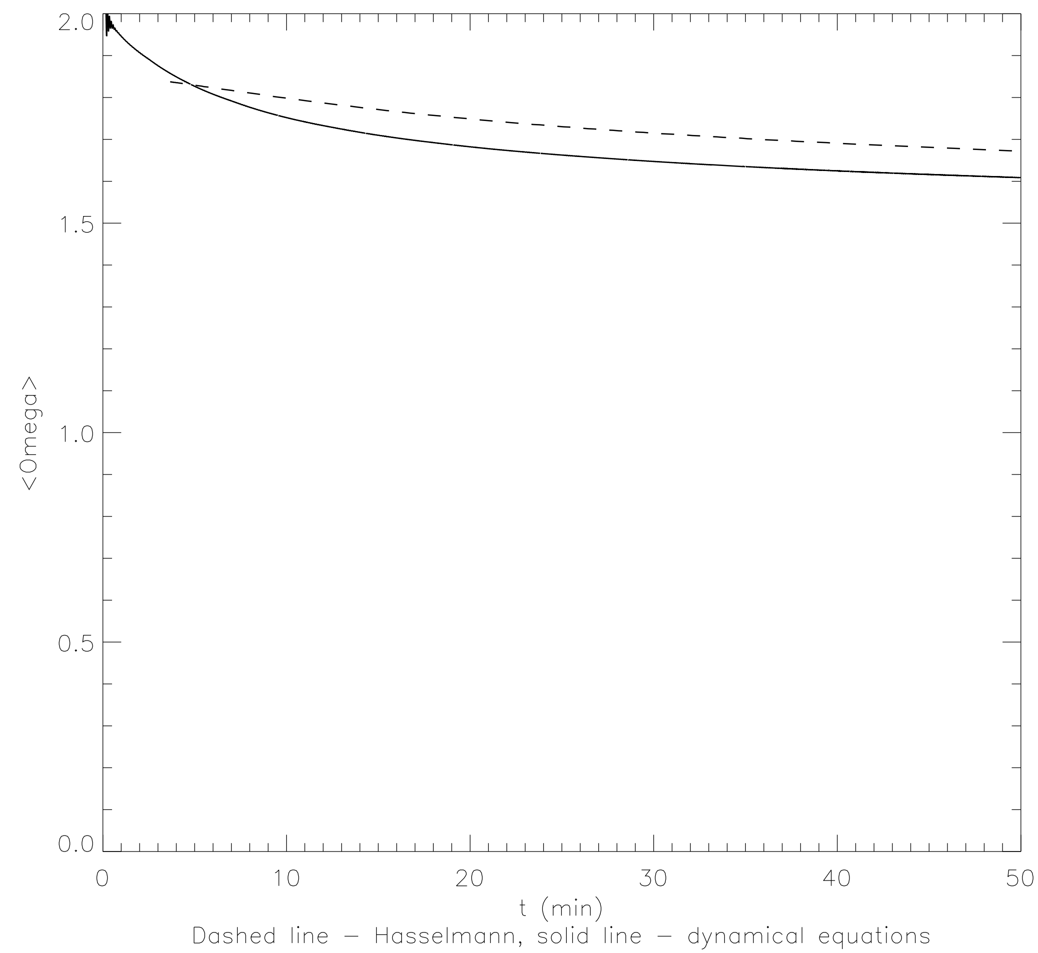

Figure 18: Mean wave frequency as a function of time for $WAM1$ case.

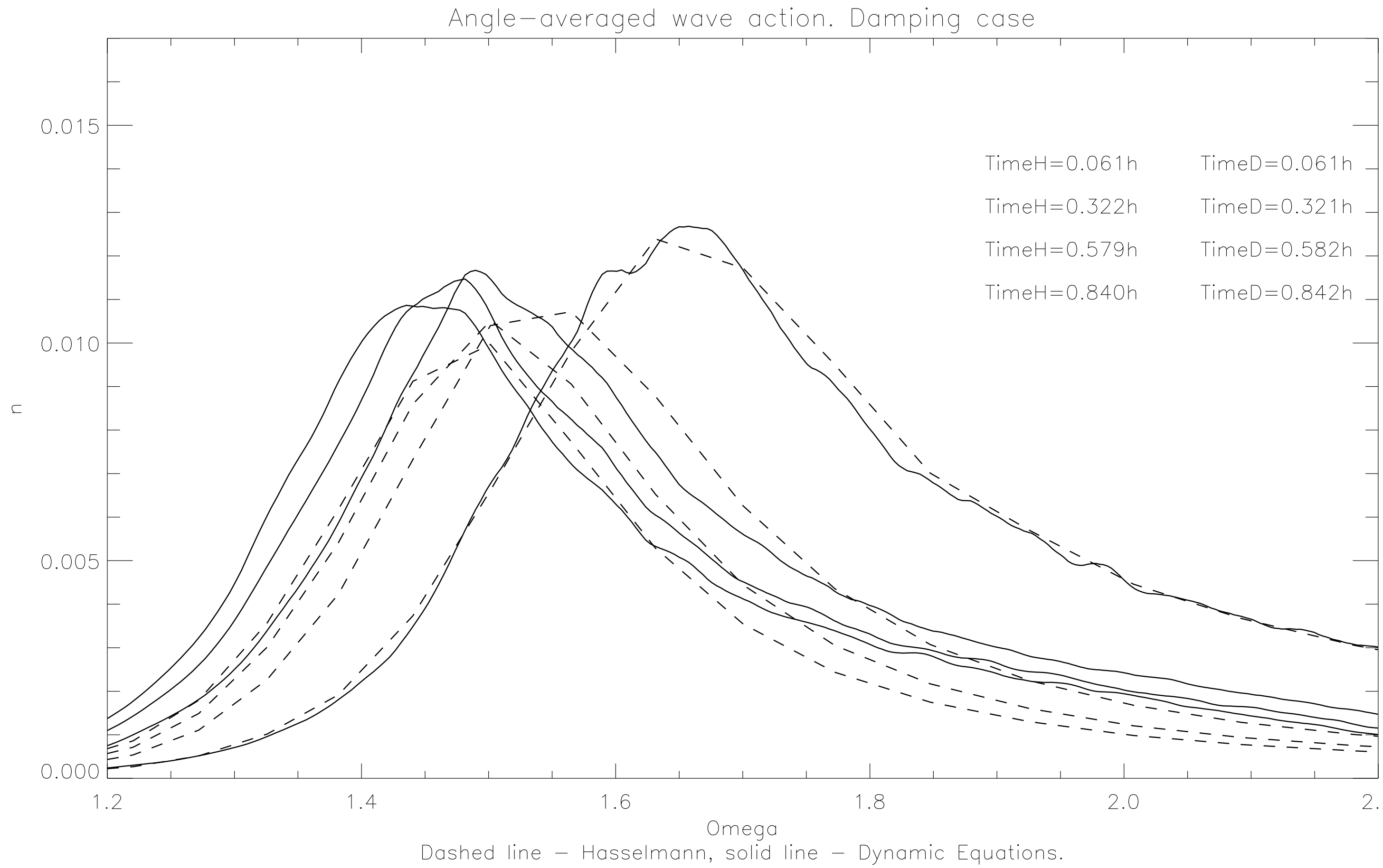

Figure 19: Angle-averaged spectrum as a function of time for dynamical and Hasselmann equations a function of time for WAM2 case.

Numerical Verification of the Hasselmann equation.

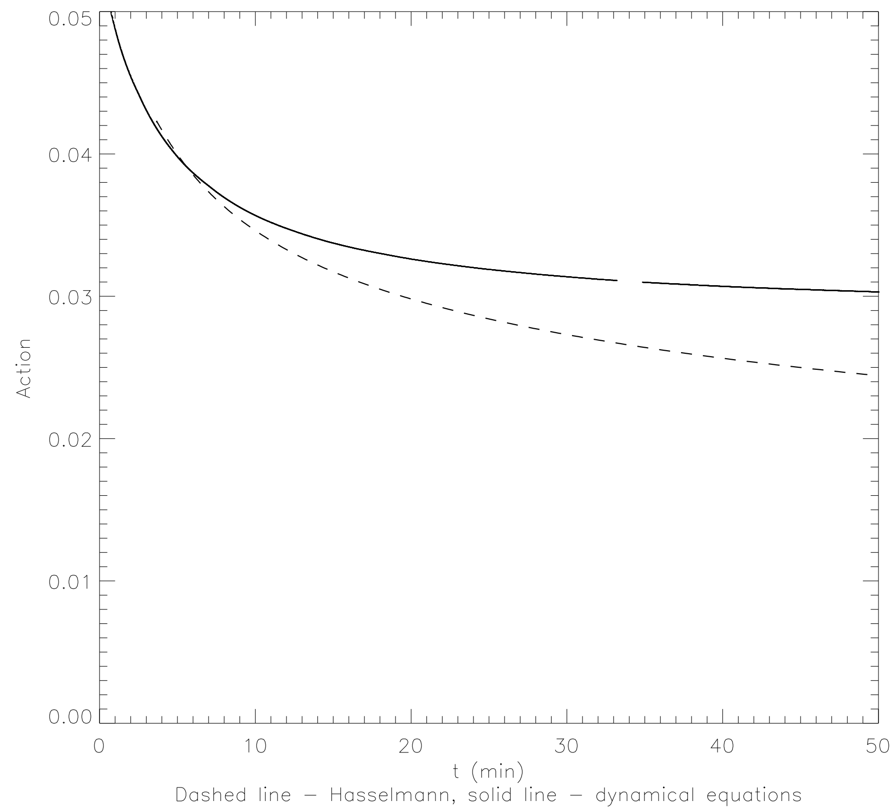

Figure 20: Total action as a function of time for $WAM2$ case

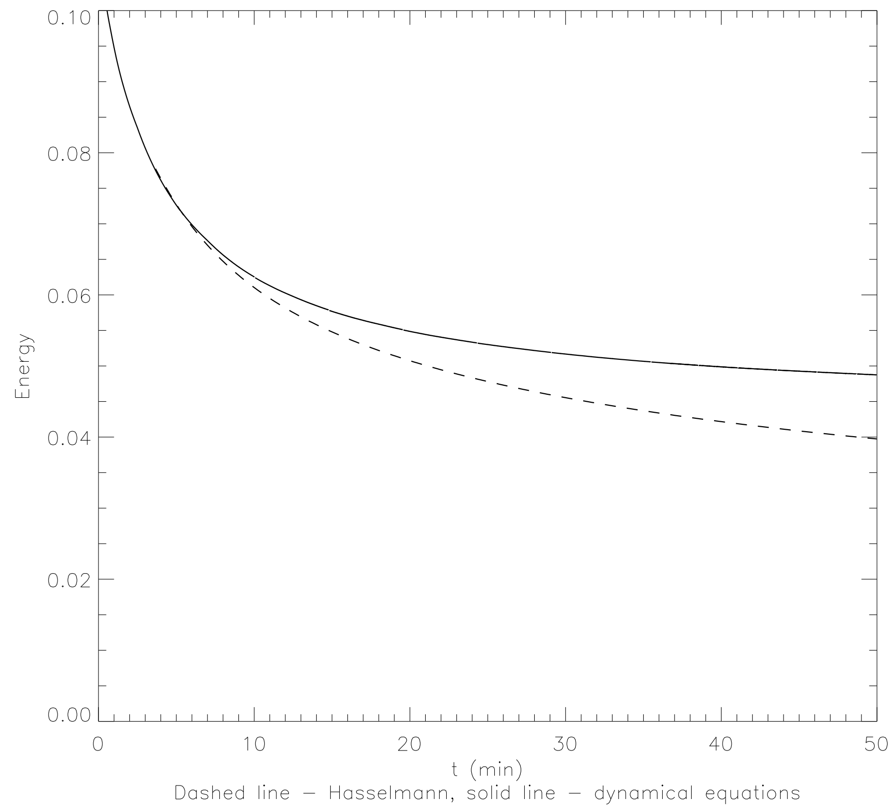

Figure 21: Total wave energy as a function of time for $WAM2$ case

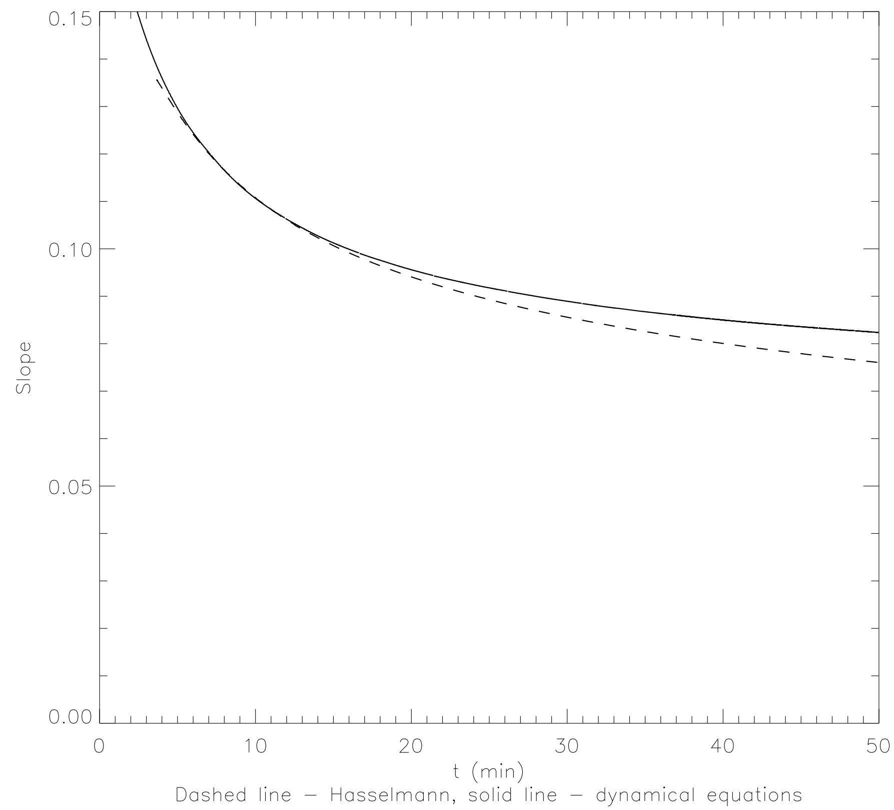

Figure 22: Average waves slope as a function of time for $WAM2$ case

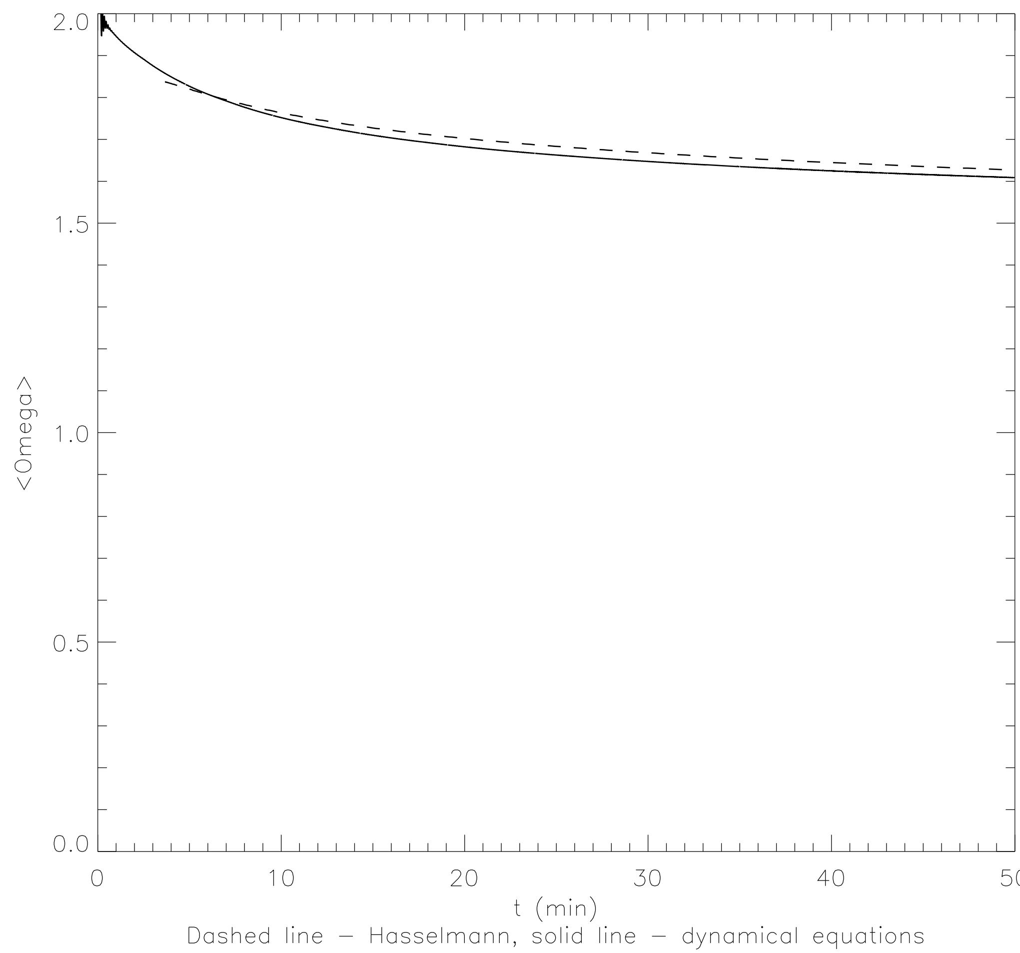

Figure 23: Mean wave frequency as a function of time for $WAM2$ case.

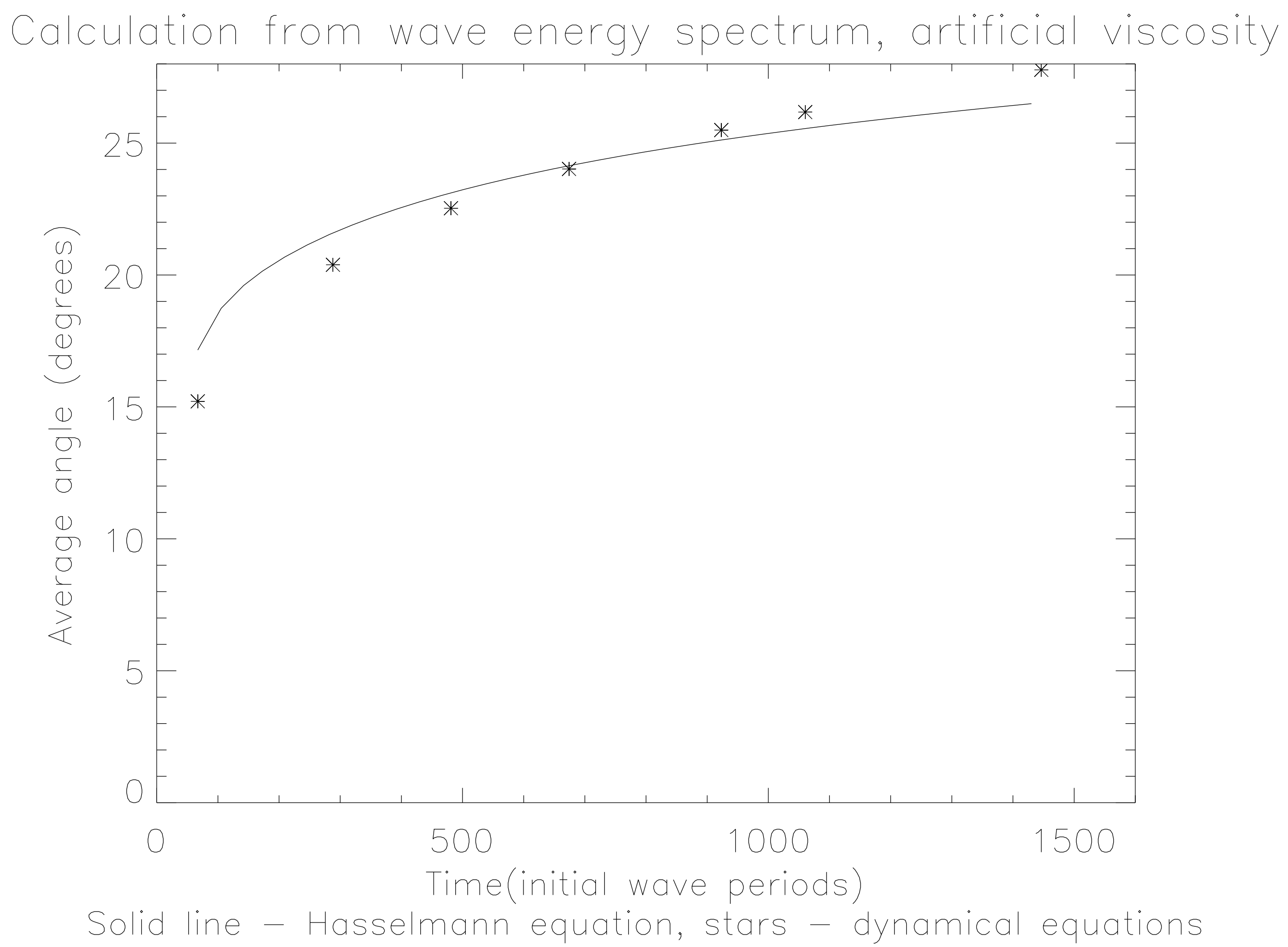

Figure 24: Energy spectrum spreading.

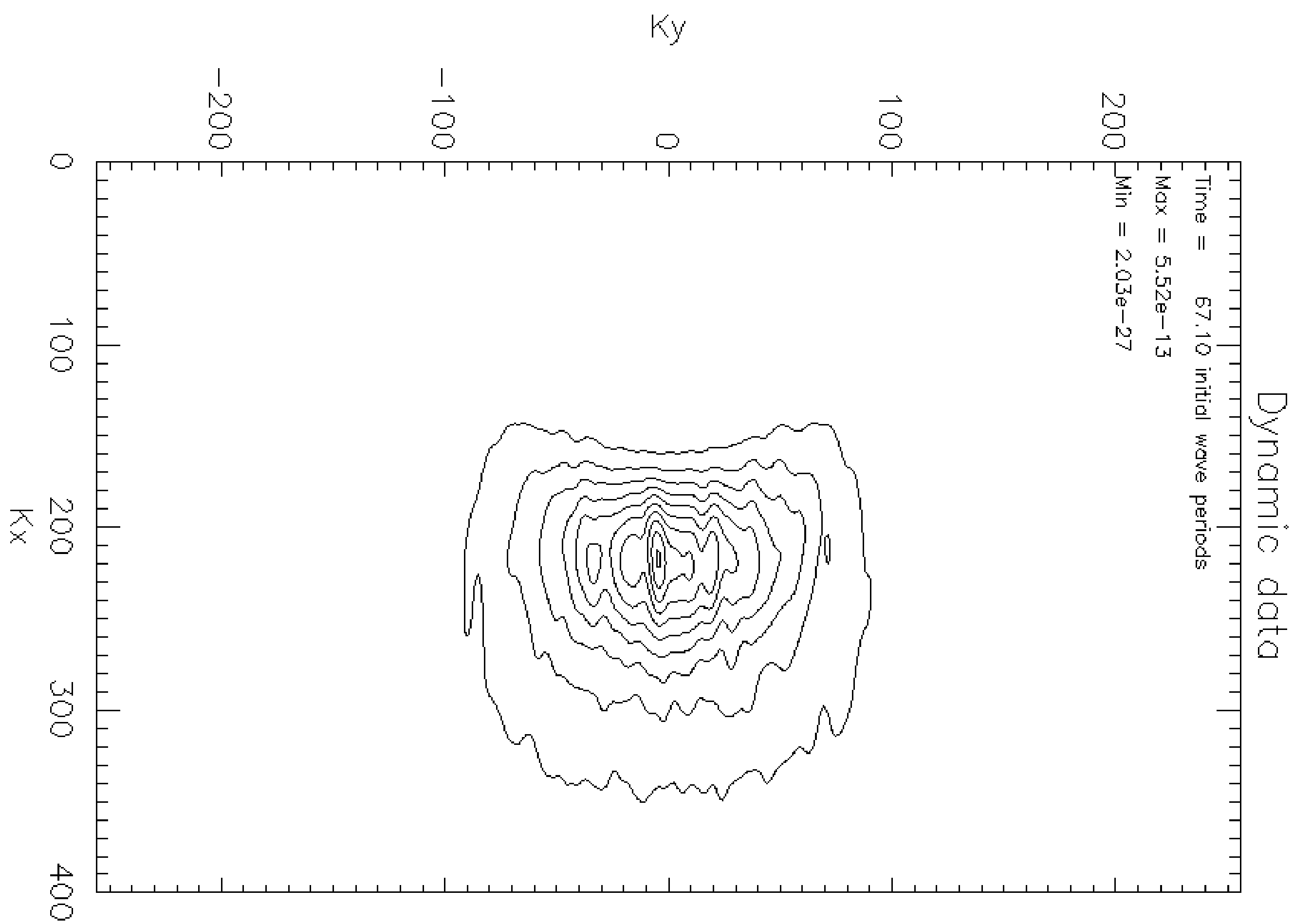

Figure 25: Isolines of the spectrum. Dynamical equations. $t = 67T_0$.

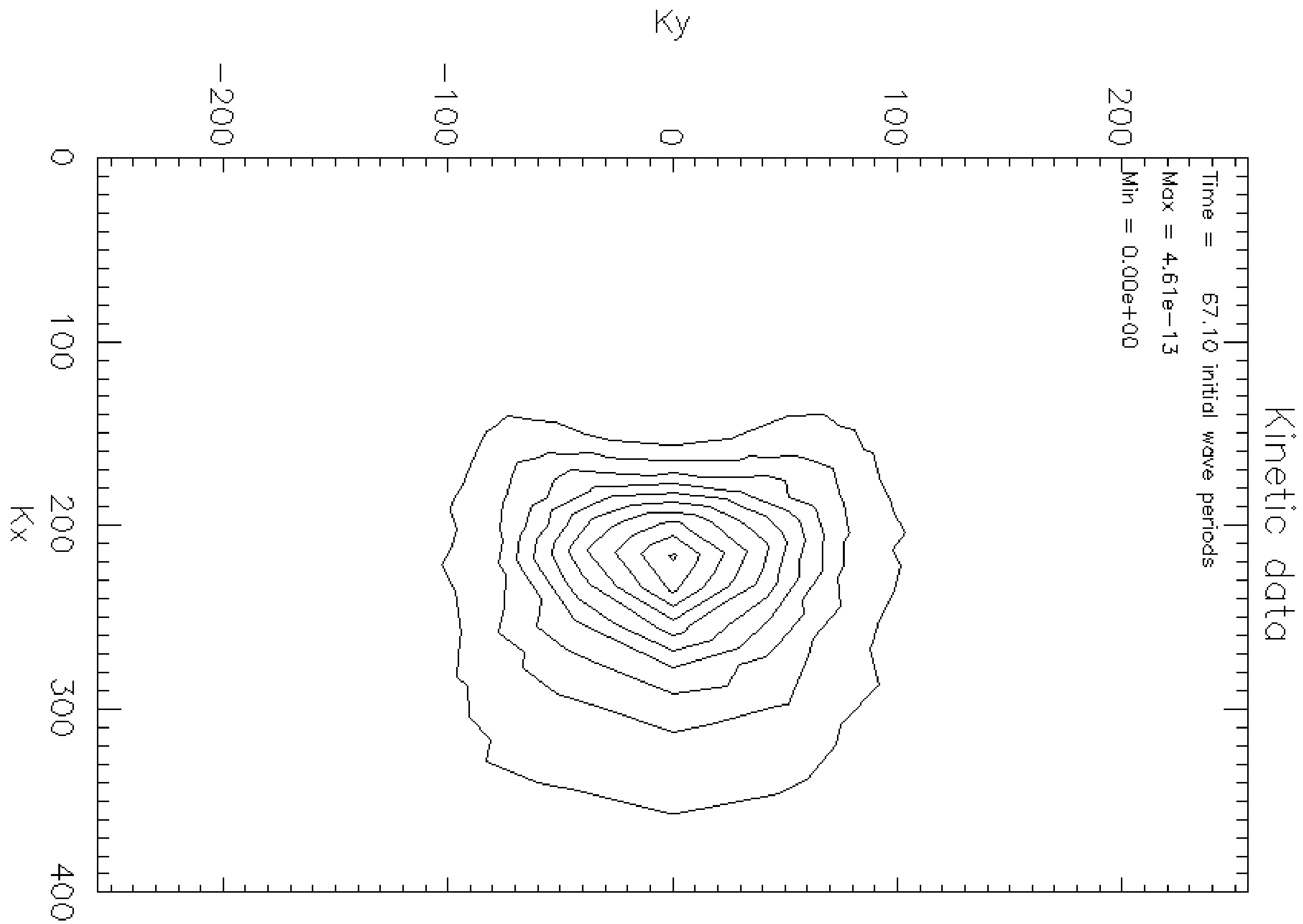

Figure 26: Isolines of the spectrum. Hasselmann equation. $t = 67T_0$.

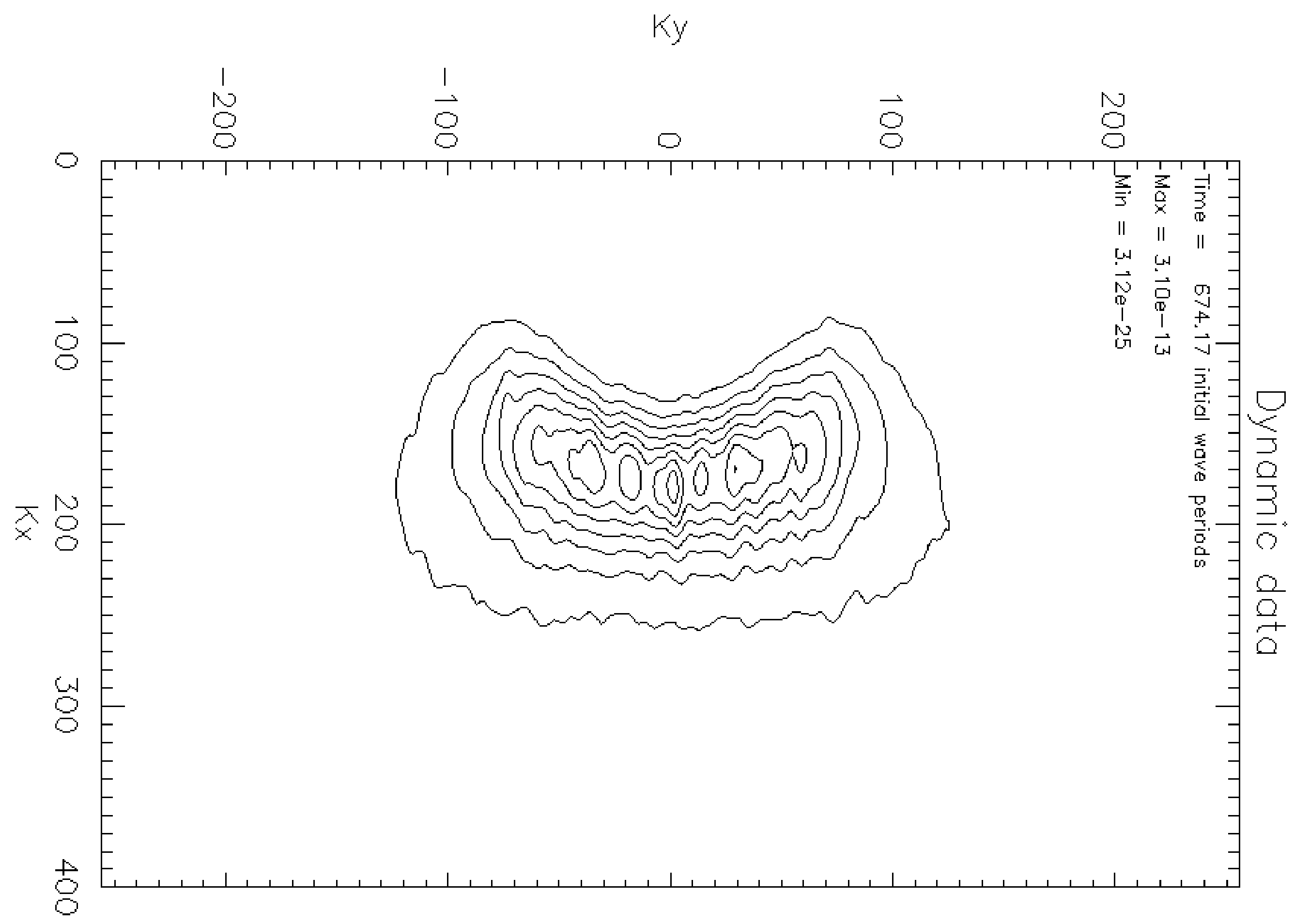

Figure 27: Isolines of the spectrum. Dynamical equations. $t = 674T_0$.

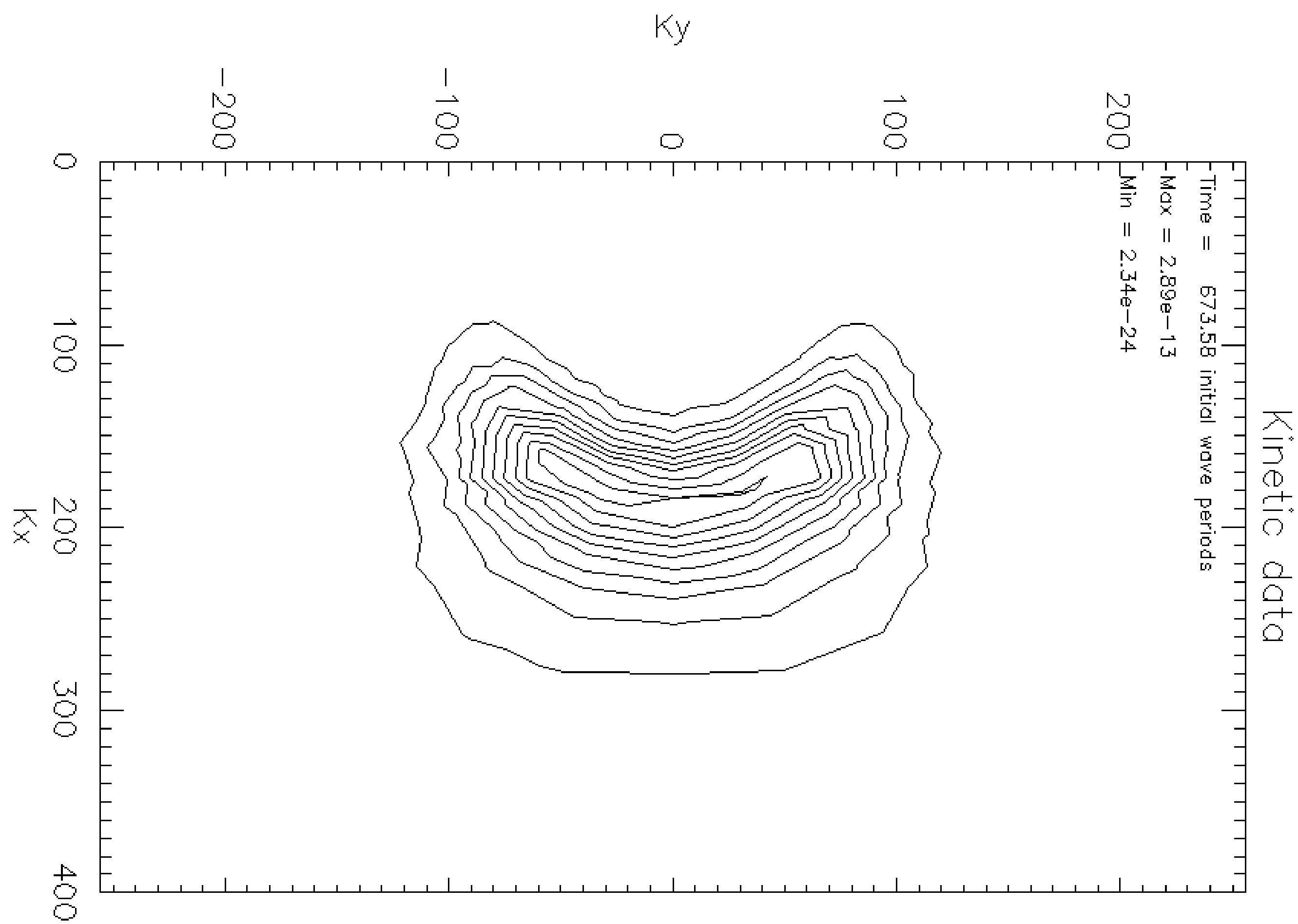

Figure 28: Isolines of the spectrum. Hasselmann equation. $t = 674T_0$.

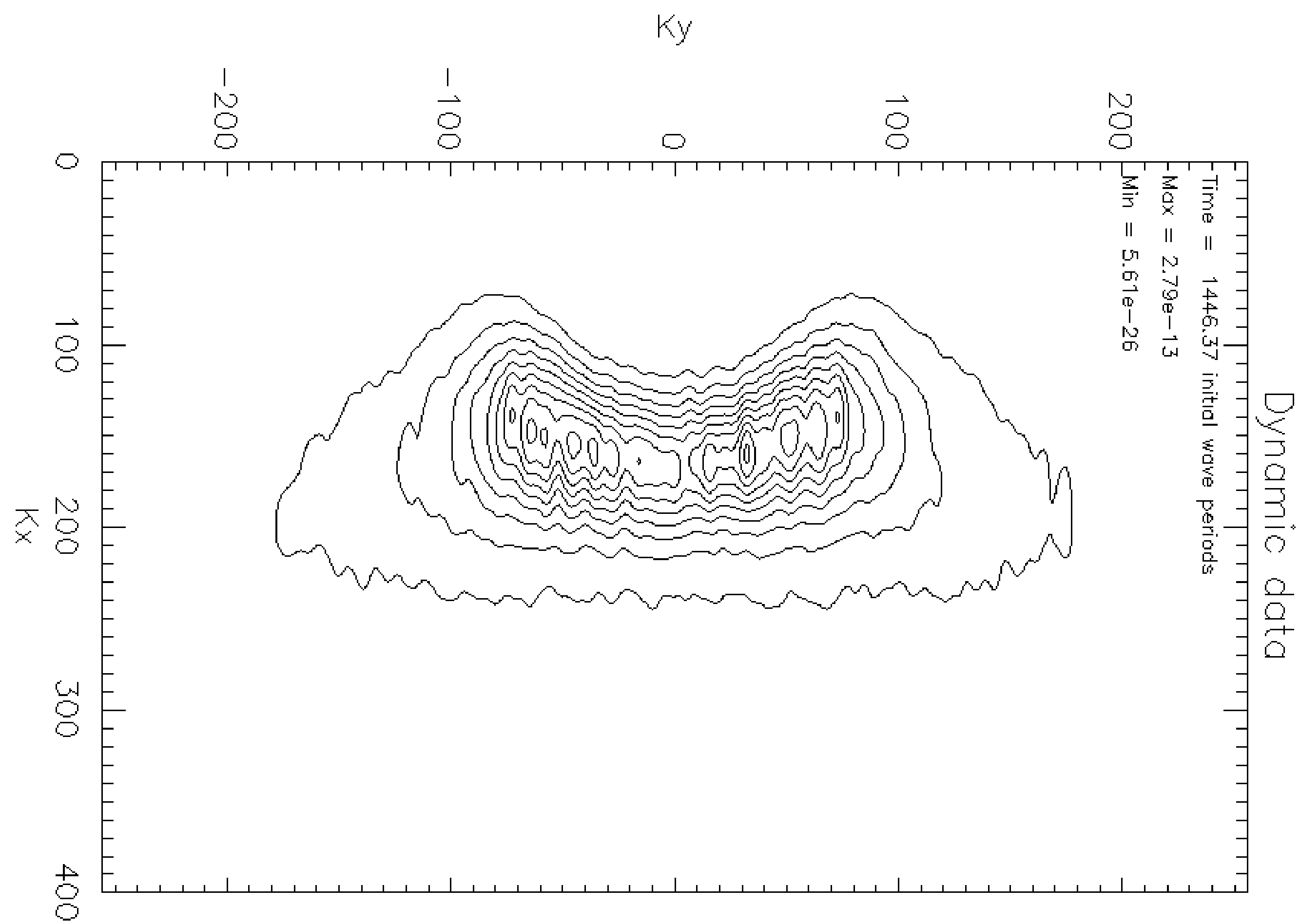

Figure 29: Isolines of the spectrum. Dynamical equations. $t = 1447T_0$.

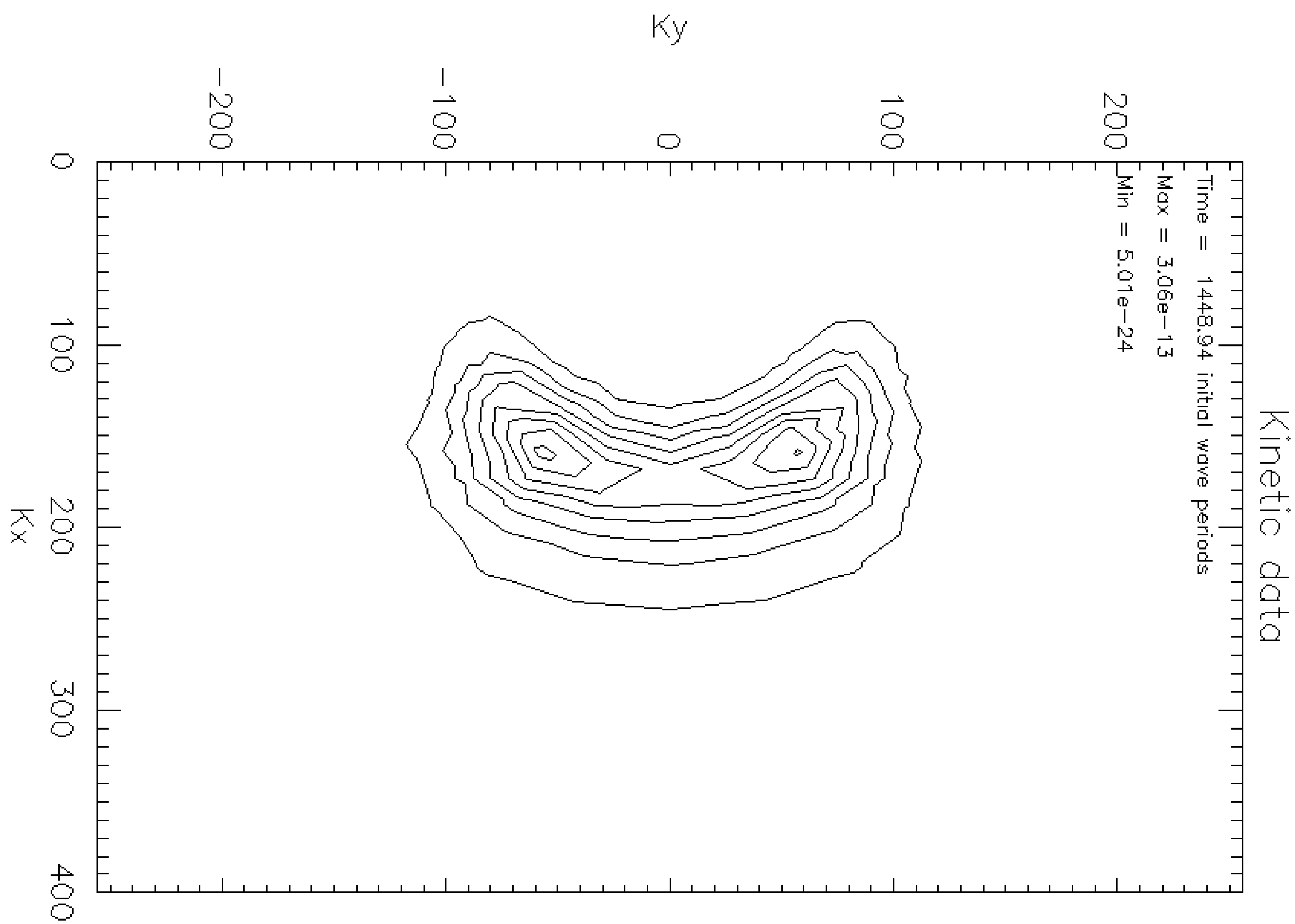

Figure 30: Isolines of the spectrum. Hasselmann equation. $t = 1447T_0$.

Inverse cascade. Frequency spectrum of action point. Dynamical equations

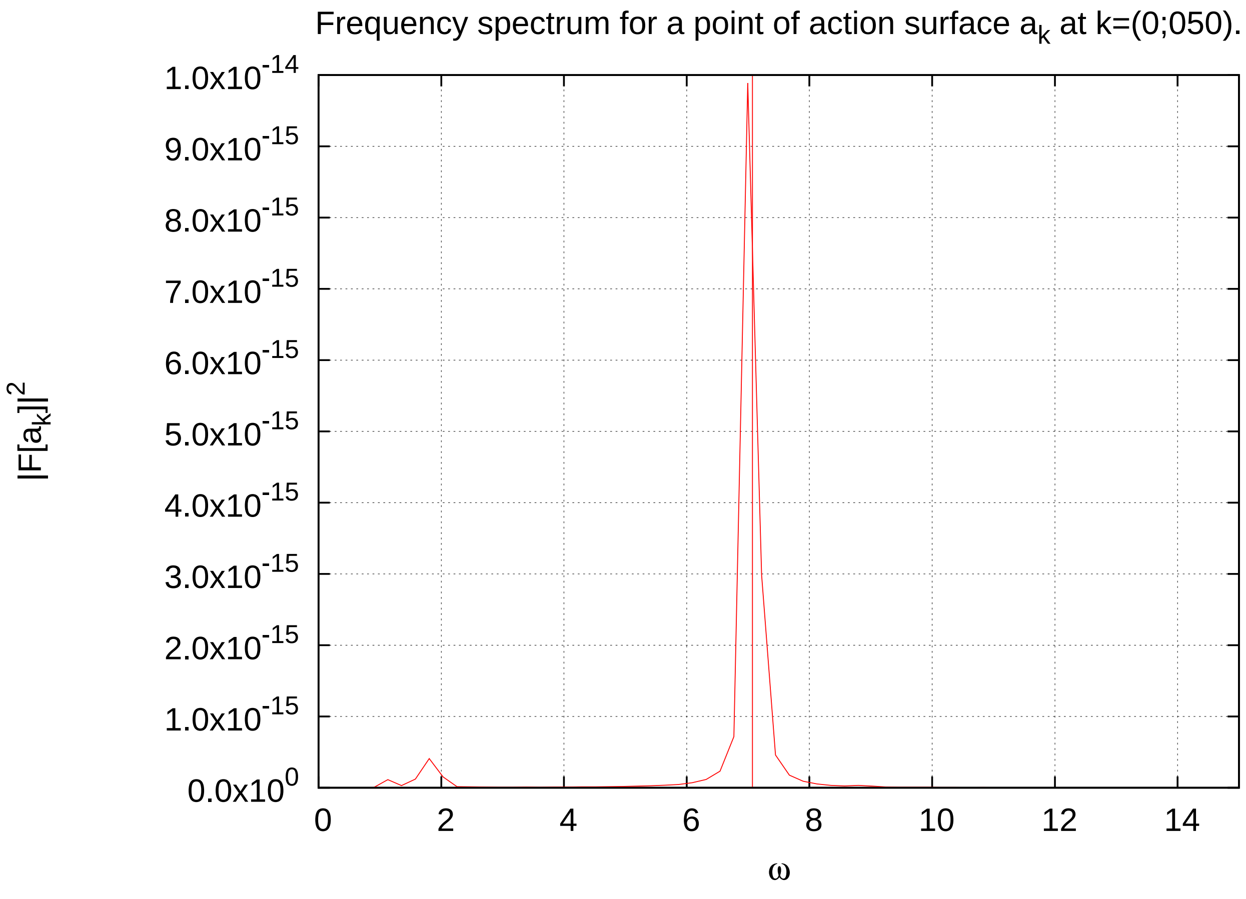

Inverse cascade. Frequency spectrum of action point. Dynamical equations

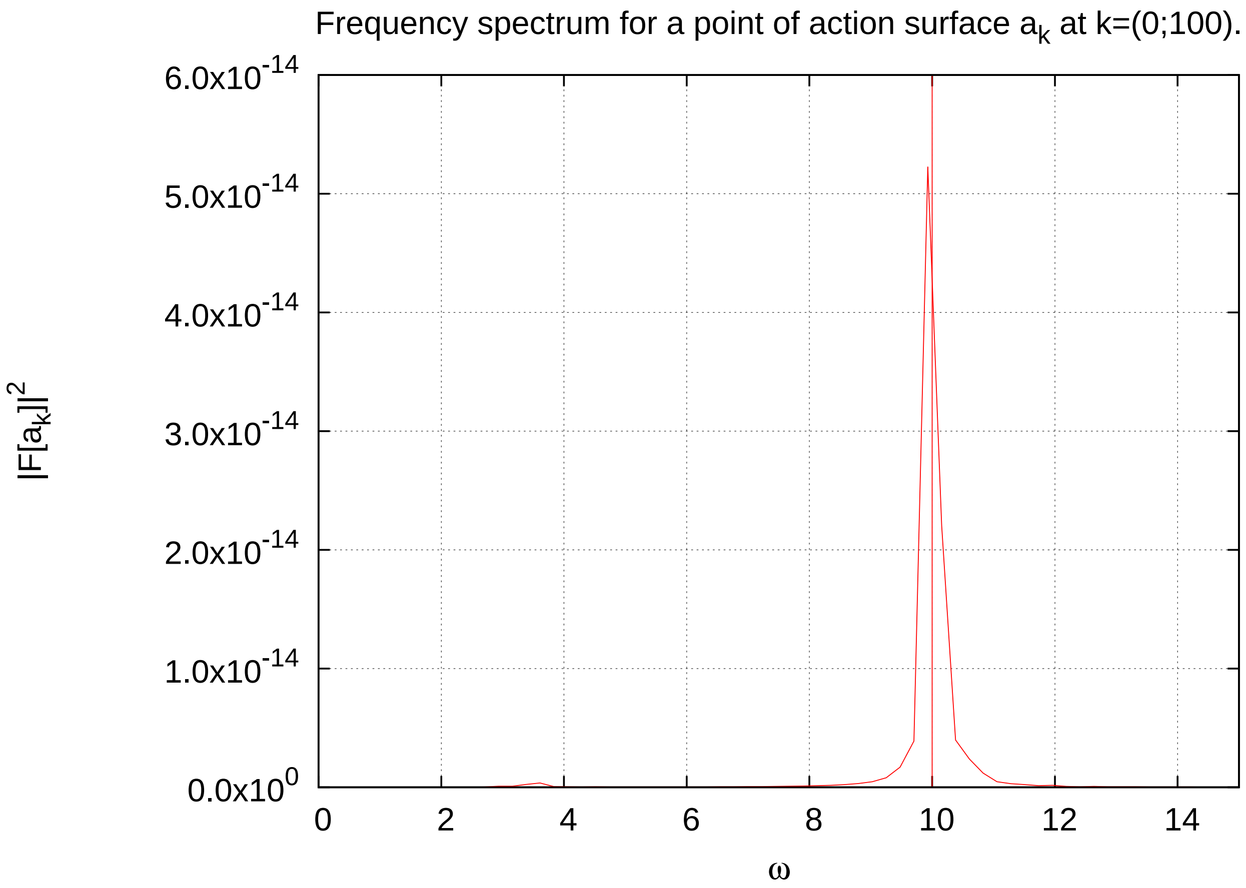

Inverse cascade. Frequency spectrum of action point. Dynamical equations

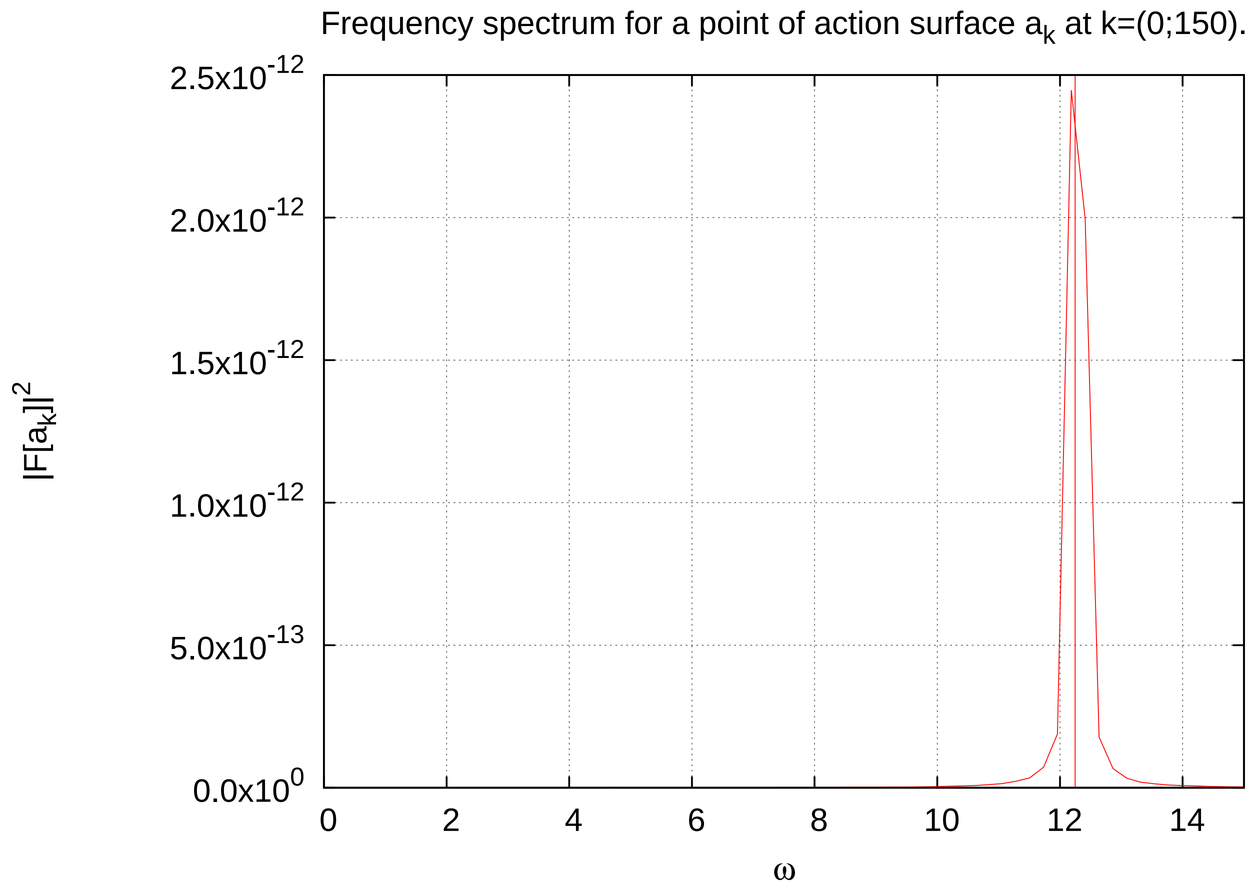

Inverse cascade. Frequency spectrum of action point. Dynamical equations

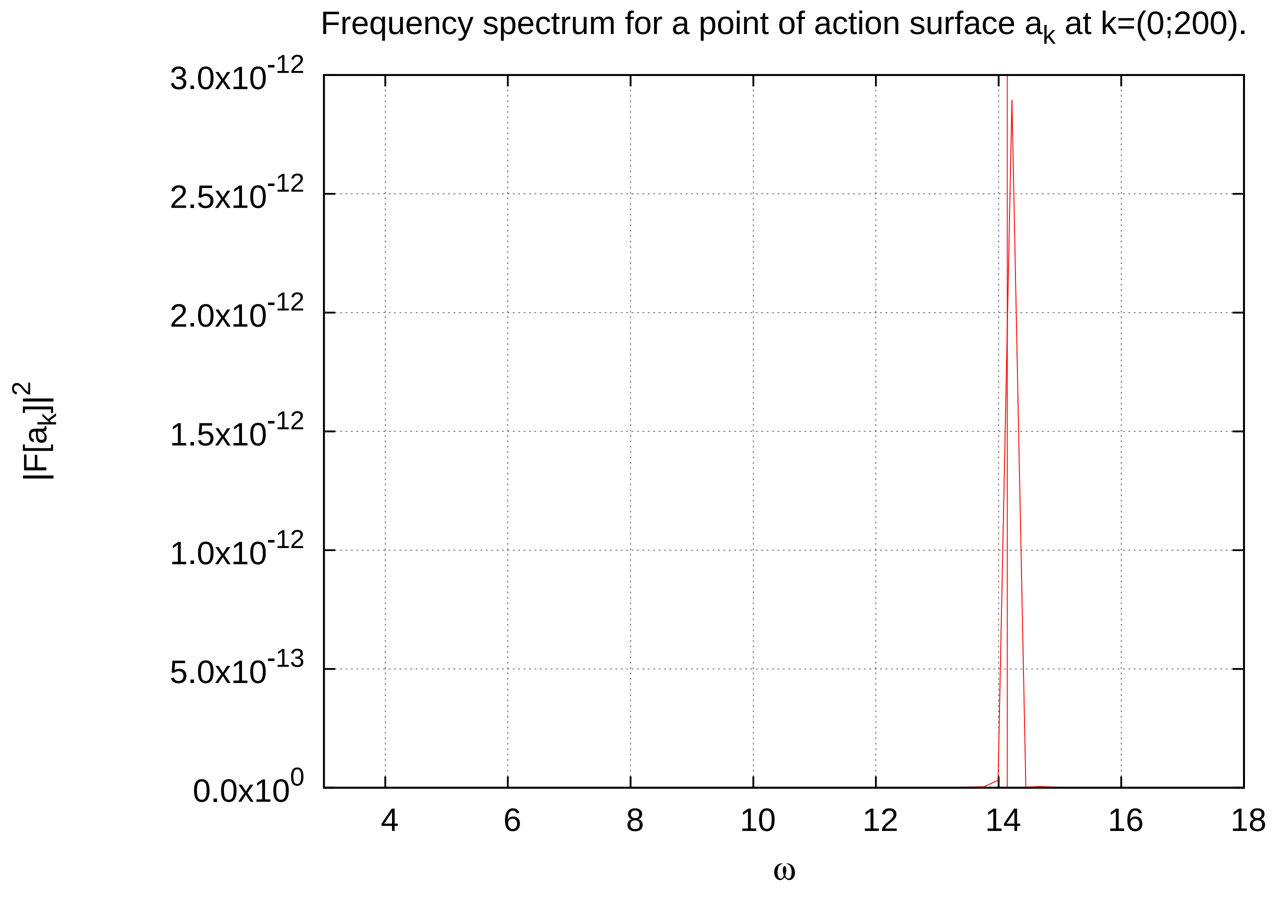

Inverse cascade. Frequency spectrum of action point. Dynamical equations

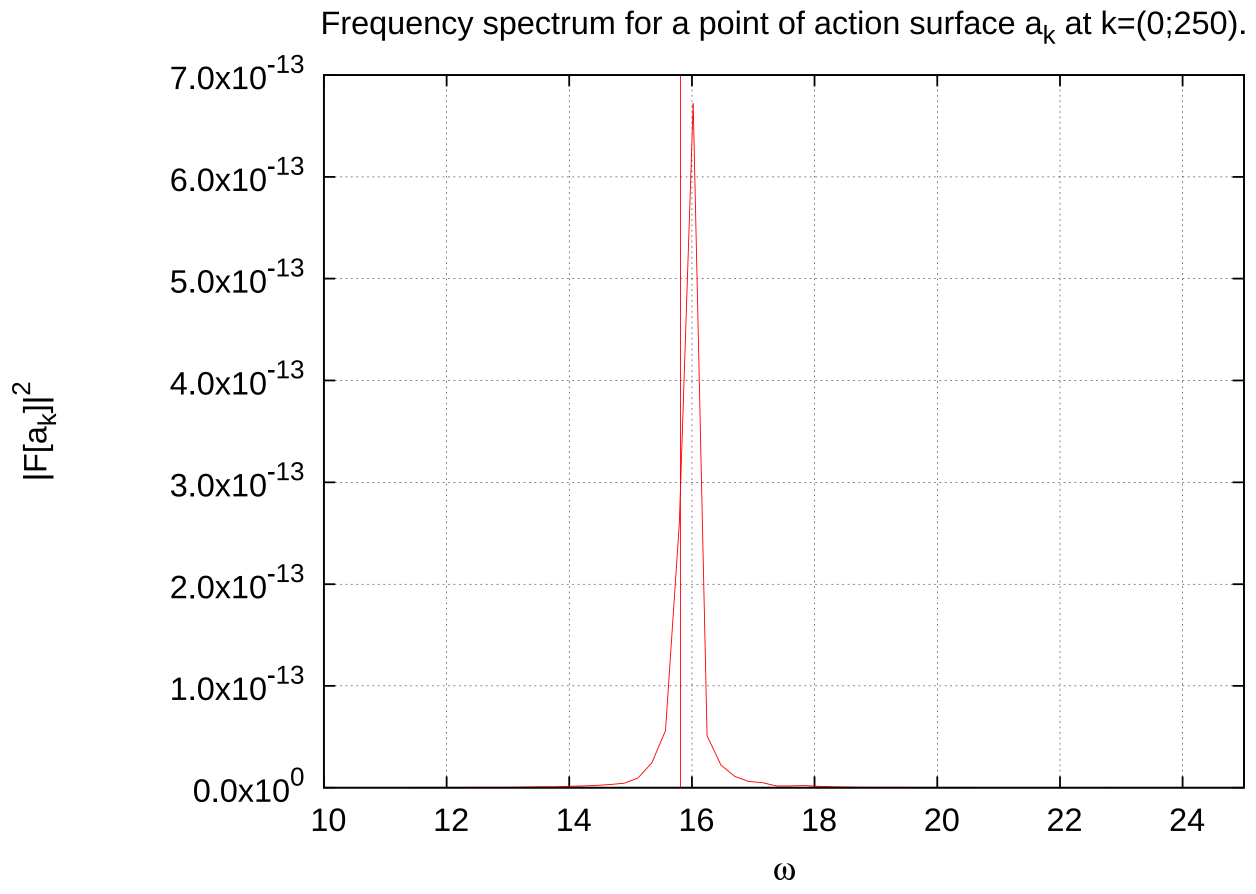

Inverse cascade. Frequency spectrum of action point. Dynamical equations

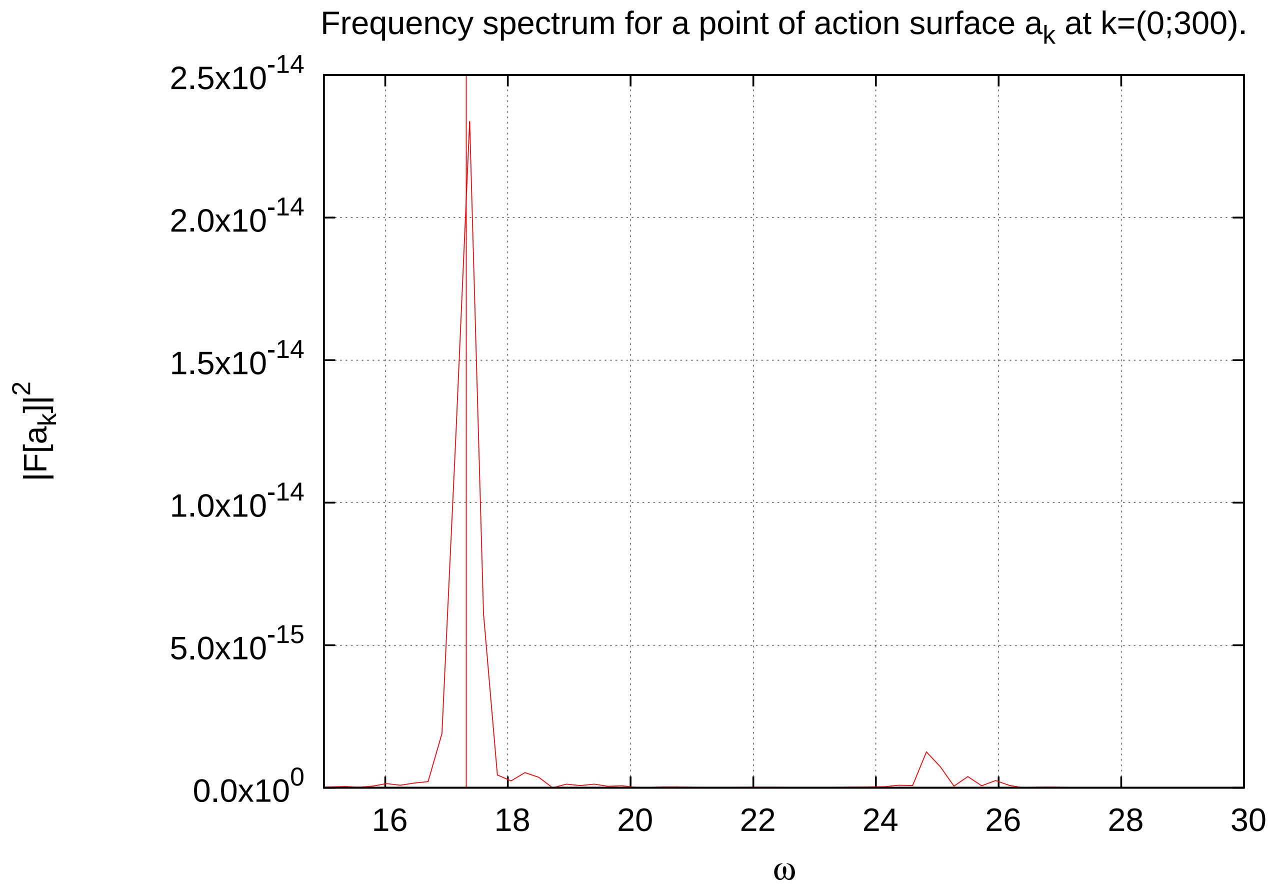

Inverse cascade. Frequency spectrum of action point. Dynamical equations

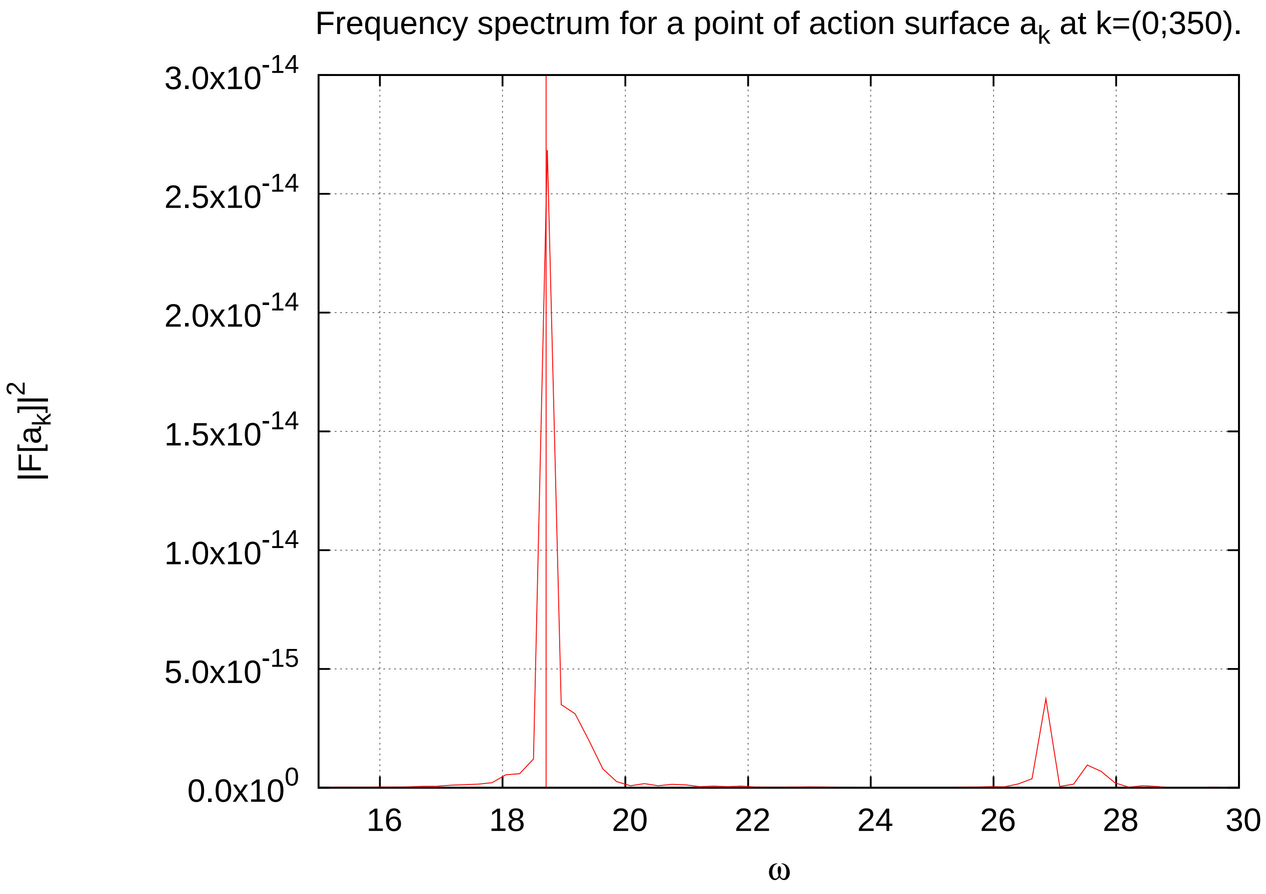

Inverse cascade. Frequency spectrum of action point. Dynamical equations

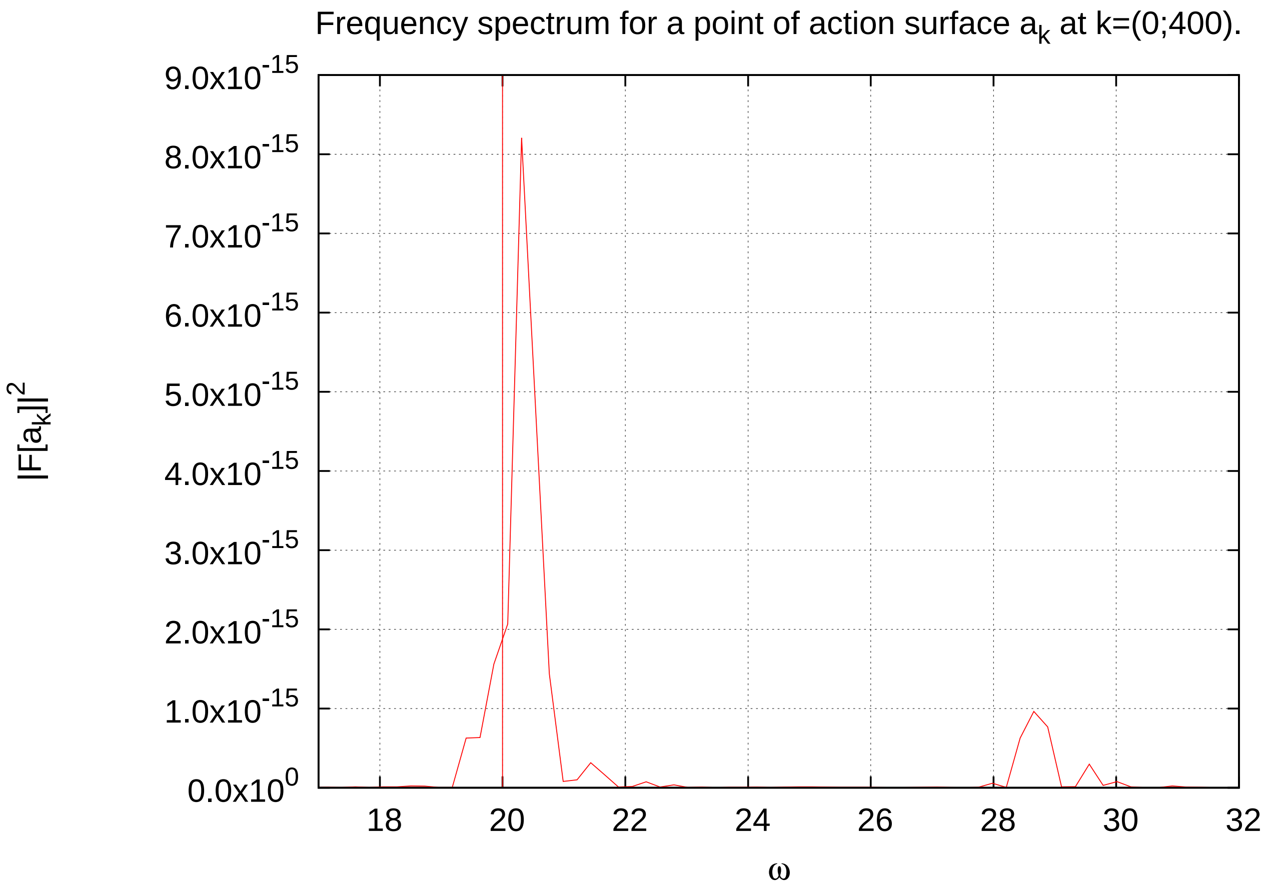

Inverse cascade. Frequency spectrum of action point. Dynamical equations

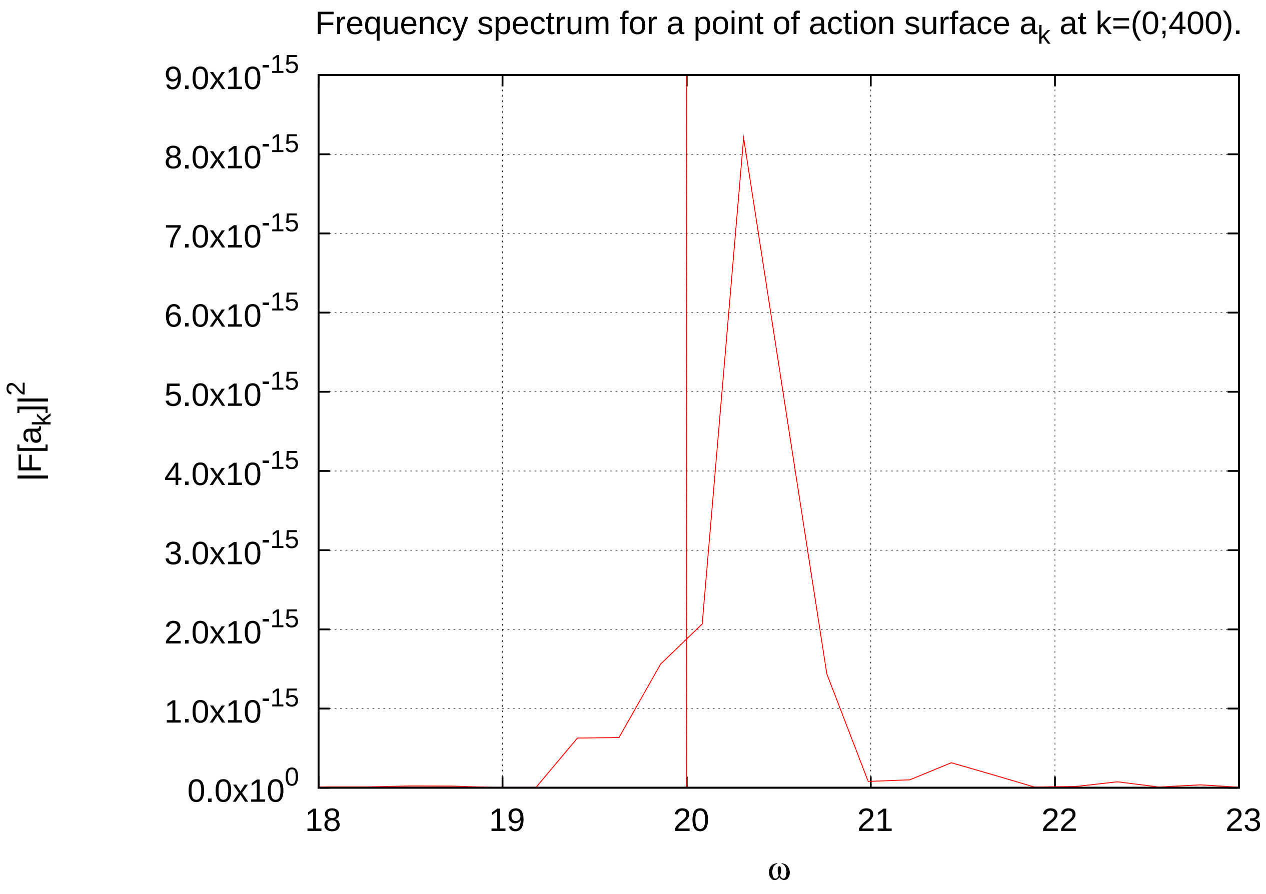

Inverse cascade. Frequency spectrum of action point. Dynamical equations